EXPERIMENTS FOR THE MEASUREMENT OF LNG MASS BURNING RATES

A Thesis

by

LADY CAROLINA HERRERA GOMEZ

Submitted to the Office of Graduate Studies of
Texas A&M University
in partial fulfillment of the requirements for the degree of

MASTER OF SCIENCE

May 2011

Major Subject: Safety Engineering

EXPERIMENTS FOR THE MEASUREMENT OF LNG MASS BURNING RATES

A Thesis

by

LADY CAROLINA HERRERA GOMEZ

Submitted to the Office of Graduate Studies of
Texas A&M University
in partial fulfillment of the requirements for the degree of

MASTER OF SCIENCE

Approved by:

Chair of Committee,	M. Sam Mannan
Committee Members,	Eric Petersen
	Kenneth R. Hall
Head of Department,	Michael Pishko

May 2011

Major Subject: Safety Engineering

ABSTRACT

Experiments for the Measurement of LNG Mass Burning Rates. (May 2011)
Lady Carolina Herrera Gómez, B. S., Universidad Industrial de Santander
Chair of Advisory Committee: Dr. M. Sam Mannan

Liquefied Natural Gas (LNG) is a commonly used flammable fuel that has safety concerns associated with vapor dispersion and radiation emitted from pool fires. The main objective of this effort is to advance the knowledge of pool fires and to expand the data that is commonly used to validate semi-empirical models. This includes evaluation of the methods that are utilized to obtain experimental values of mass burning rates, which are used in models where semi-empirical correlations cannot be applied.

A total of three small-size experiments designed to study the radiative characteristics of LNG pool fires were carried out at Texas A&M University's Brayton Fire Training Field (BFTF). This set of experiments was designed to study how the heat feedback from the fire to the pool surface is subsequently distributed through the liquid volume and the validity of different methods for measuring burning rates. In this work, a number of semi-empirical correlations were used to predict the characteristics of the flame and examine the predictive accuracy of these correlations when compared to the values obtained experimentally. In addition, the heat transferred from the energy received at the pool's surface to the surroundings was investigated. Finally, the parameters that influenced the measurement of radiative head feedback to the liquid pool were analyzed to investigate potential causes of calibration drift in the instrumentation.

The results of this work provided information regarding the validity of certain techniques for the measurement of mass burning rates and the use of correlations to predict the characteristics of an LNG pool fire on a small-scale. The findings from this work indicate that the energy received at the liquid surface was used entirely for evaporation and no indications of transmission to the surroundings were observed. Lastly, it was found that during the experiments, the sink temperature of the sensor was not constant, and therefore, the readings of the radiative heat were unreliable. This was due to the insufficient cooling effect of the water circulated. It was later shown in the laboratory that through a series of qualitative tests, a change of 20℃ in the cooling water resulted in a calibration drift.

ACKNOWLEDGEMENTS

I would like to thank Dr. Sam Mannan for his support and guidance through my graduate studies. His advice and challenging discussions motivated my interest in the area of Process Safety and will always be present in my professional career. I would also like to thank Dr. Ray Mentzer whose advice and guidance contribute to the success of this work. I would like to acknowledge my committee members, Dr. Petersen and Dr. Hall. I would also like to express my gratitude to Dr. Phani Raj and Dr. Hans Pasman for sharing their vast experience and knowledge, and their time. Their comments were greatly appreciated. I would like to thank previous and the current Liquefied Natural Gas (LNG) team, whose help and efforts permitted the completion of the field tests. I would like to express my thanks to Kirk Richardson and the team of firefighters present during the tests that permitted their safe execution. Finally, I would also like to thank the Mary Kay O'Connor Process Safety Center (MKOPSC) staff and students for their support.

TABLE OF CONTENTS

Page

Page

LIST OF FIGURES

Page

Page

LIST OF TABLES

Page

1. INTRODUCTION*

1.1 LNG background

Liquefied Natural Gas (LNG) is a mixture of hydrocarbons, in which methane gas is the main component (>90%). The liquefaction of this gas can be carried out either by cooling it down to 111K at ambient pressure or pressurizing it at ambient temperature. This process reduces the space occupied by 1/600 of the space used by the gas. This results in a relatively clean energy source and a cost-effective alternative for transportation, distribution, and storage. Increasing demand has made the technology and process involved in the production of LNG widely characterized and continuously investigated to create safer operation conditions. Thus, LNG is a feasible alternative to other fuel sources, such as coal and renewable resources, from economic, environmental and safety perspectives [1].

Natural gas is growing in demand; unfortunately some gas reserves are stranded without a pipeline for distribution. Therefore, a convenient way to transport natural gas is by converting it to LNG. This involves a number of stages such as liquefaction where LNG will be produced, storage, loading/unloading, transportation, regasification where natural gas is obtained, and finally distribution in gaseous form.

This thesis follows the style of the *Journal of Hazardous Materials*.

*Part of this work is reprinted from *Experiments for the measurements of LNG mass burning rates*, Carolina Herrera, Ray Mentzer, and M. Sam Mannan, Submitted to Journal of Loss Prevention in the Process Industries.

1.1.1 Demand for LNG

According to the Energy Information Administration, EIA, the demand for natural gas in the U.S. as an energy source will continue to increase 20% in the upcoming 20 years as shown in Figure 1. Nearly 24% of the overall energy used in the United States (U.S.) comes from natural gas. Globally, most new power plants are fueled by natural gas. LNG is a sound option for meeting increasing global natural gas demand. LNG imports have become a viable option, projected to continue growth through 2030 [2].

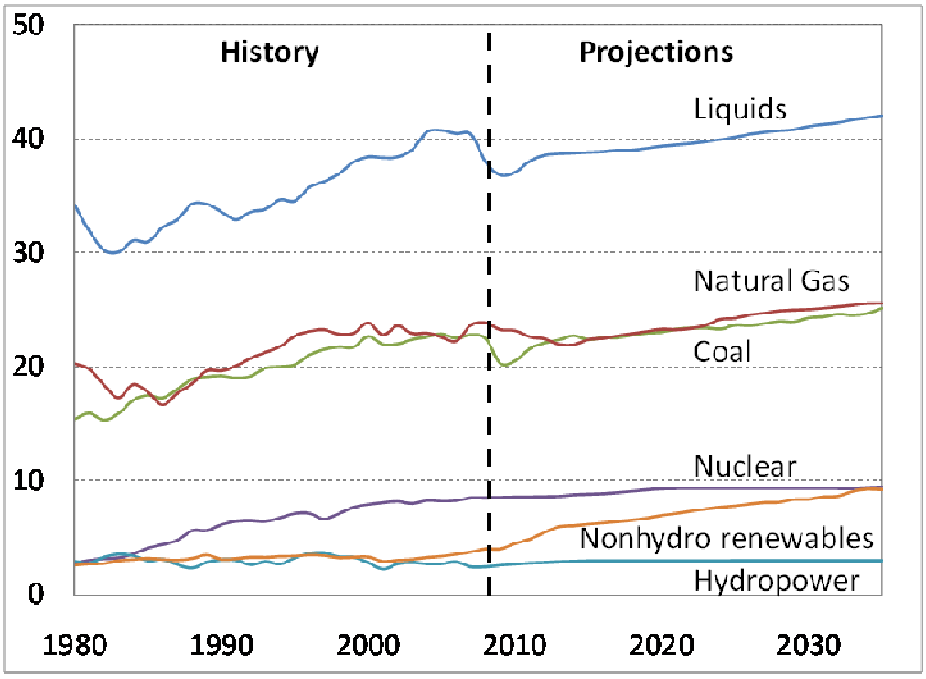

Figure 1. U.S. Energy consumption by fuel [2]

By September 2002, about 113 facilities were reported to be operating in the U.S., including maritime terminals and “peak-shaving” facilities used to meet the demand-supply year round. Currently in the U.S., 9 LNG terminals, both offshore and onshore, are operating. Pursuit of other proposed projects will depend on the anticipated supply and price of natural gas, which has recently

been impacted by the discovery of plentiful domestic coal-bed methane resources.

1.1.2 Hazards

LNG is an odorless, clear, non-corrosive, non-toxic, asphyxiant, flammable liquid at cryogenic temperatures. As with other materials, there are a number of potential hazards associated with the use of LNG [3-4].

- Humans can get freeze burns and/or potential asphyxiation.
- Embrittlement is a known outcome for some metals due to the thermal shock when exposed to low temperatures for prolonged times.
- Pool fire: occurs when liquid LNG is spilled on the ground or on water and ignited.
- Jet fire: occurs when a leak from a pressurized container is ignited.
- Cryogenic hazards: occur from the thermal characteristics of this cryogenic fluid.
- Flash fire: occurs when flammable vapors are not ignited immediately after the release, but instead, a vapor cloud forms, ignites, and burns back to the leak source. This type of combustion does not create significant overpressure.
- Vapor cloud explosion: occurs when a vapor cloud burns resulting in appreciable overpressure.
- Rapid phase transition: occurs when a release on water vaporizes too fast, which does not allow sufficient time for separation of the water-LNG mixture. This phenomenon occurs due to the difference in densities, and resembles a flameless explosion.

1.2 Motivation

The future development and operation of LNG facilities brings safety concerns related to the potential consequences of a release and subsequent ignition. Legislative efforts have been put in place since the 70's to regulate and provide good practices for the safe operation of the LNG industry. *NFPA-59 Standards for the Production, Storage, and Handling of Liquefied Natural Gas* [5] deals with LNG facility layout and includes the heat flux value of 5 kW/m^2 as a design criterion. In the U.S., $5kW/m^2$ is used as a rule of thumb to define the maximum radiation that a person can be exposed to in 20 seconds, and therefore is set as the limiting edge of the exclusion zone. Exclusion zones are defined as the distance from a fire at which the thermal radiation can cause harm to people or structures. Distances beyond this boundary are considered to be safe. Other regulations such as *49-CFR-193 Liquefied Natural Gas Facilities: Federal Safety Standards* [6] are concerned with facility siting, and specifically require the prediction of hazardous distances based on thermal radiation for siting of onshore regasification terminals.

Previous research has focused on the consequences of thermal radiation arising from a pool fire without detailed information on the role played by the liquid and gas formed. Moreover, key parameters used to describe thermal hazard zones have been calculated based on semi-empirical data without regard to the optical properties involved in this phenomenon or through field models whose variables have been validated over only a limited range. Results reported by Malvos and Raj [7-8] have highlighted the importance of a clear description of the fundamental parameters involved in the calculation of hazard zones: pool geometry, mass burning rate, and Surface Emissive Power (SEP).

In 1987, a series of tests was performed at the Gaz de France (GdF) test facility in Montoir, France. Mass burning rates were calculated through two approaches: using helium-purged dip tubes to directly obtain the mass

evaporated and indirect calculations of the mass rate given the measured radiative heat reaching the pool [7, 9-10]. Possible explanations of the overestimation obtained from the indirect calculations include: the absorption of energy by the cold soot found at the bottom section of a large scale LNG pool fire; absorption and scattering of the energy by the droplets that originate from the boiling of the liquid and the fuel gas found on the pool surface; and the reflection and transmission of energy by the liquid surface to the bottom of the pool and the surroundings [7, 11]. These methods disagree by a factor of 2.5 and raised questions regarding the methodology used and the validity of the assumptions commonly accepted in the calculations.

1.3 Problem statement

The thermal characterization of a pool fire involves a number of variables that influence the predictions made when using the developed models. Mass burning rates can be measured or estimated either by experiments or by the use of computational or semi-empirical models. Clearly, the impact of this variable was observed in the Montoir tests where over-prediction of exclusion zones could have been the result of an erroneous value for the mass burning rate input in the thermal radiation calculation. Thus, an accurate estimation of mass burning rates is essential for the prediction of flame characteristics, which subsequently have a major impact on the description of thermal hazard distances, as seen in Figure 2. This figure shows the intrinsic relationship between the mass burning rates, the geometry of the flame, and the properties of the flame. It illustrates how the thermal radiation received by objects outside of the pit are influenced by the burning rates that are simultaneously dependent on the radiative heat feedback from the flame to the pool.

The prediction of the potential consequences of an LNG incident cannot rely simply on data obtained from experiments over a limited range and extrapolated based on a model's predictions [12-13]. Therefore, it is important to reevaluate the validity of semi-empirical models and to understand the fundamental behavior of LNG pool fires to properly predict the potential hazards posed by this type of scenario.

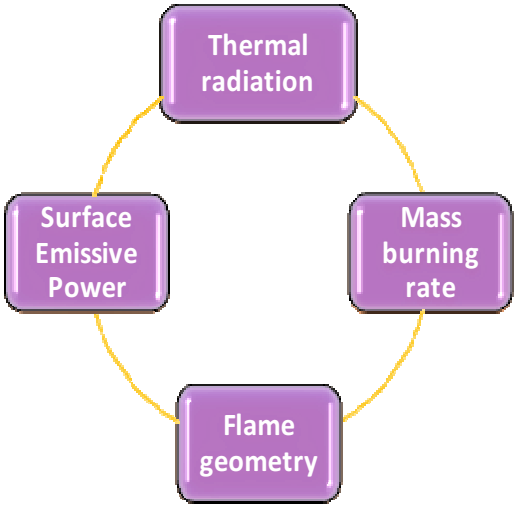

Figure 2. Relation between thermal radiation and mass burning rates

To accurately address the hazards arising from LNG pool fires, experimental and theoretical analysis needs to be performed, where the effect of the transference of heat through distinct phases of a material are accounted for when heat feedback from a flame drives the evaporation of the fuel, and therefore determines exclusion zones.

1.4 Objectives

The present work focused on improvement of the fundamental understanding of burning rates driven by radiative heat feedback under real conditions. The objectives of this work were:

- To carry out a set of tests to gather data for further analysis for the validation of the methodology commonly use in these types of experiments.
- To study the mass burning rate of LNG by using different methods commonly used in the literature.
- To measure the heat flux transfer occurring from the bottom of the pool to the liquid pool and to determine the transmission of energy perpendicular to the liquid surface.
- To analyze the parameters that could impact the measurement of heat feedback from the flame to the liquid pool when LNG vaporization rates are obtained from these values.

The outline of this work follows the proposed objectives and therefore is organized accordingly. Section 1 introduces the background for LNG pool fires and the motivation for this work. Section 2 contains supporting information for this work through literature review pertaining to the geometry, mass burning rates, and characterization of LNG pool fires. Section 3 presents the details concerning the experimental set up and the description of the tests. Section 4 provides the results obtained by incorporating the information presented in Section 2 and the data obtained through the experiment development described in Section 3. Finally, Section 5 contains a summary of the conclusions, limitations, and recommendations for future work.

2. BACKGROUND OF LNG POOL FIRES

Pool fires are formed when a released fuel that accumulates on a substrate is ignited. When the released fuel does not find an immediate ignition source, a flash fire occurs and its effects are different due to the difference in burning periods and spreading of the flames. The parameters involved in the quantification of its effects include: geometry of the flame, radiative power, and characteristics of the object of interest. Moreover, the accurate quantification of the parameters will provide a perspective of the hazards posed by this scenario.

2.1 Geometry of the flame

Parameters such as diameter, shape, height, tilt, drag, and pulsation are used to describe the flame's geometry for hydrocarbon pools. An accurate prediction of this feature provides a more credible scenario of the consequences posed by pool fires since these parameters are used in the calculation of the radiative heat emitted by fires

2.1.1 Diameter

Pool fire diameters vary in shape. A pool fire is considered to be of a regular form if it is contained and of a fixed shape; otherwise, it is considered to be of an irregular shape. For cases other than circular perimeters, it has been found that it is most suitable to calculate an equivalent diameter to be used in subsequent calculations [4, 14]. This parameter is given by:

$$D = \frac{4A_p}{S_p} \qquad 2\text{-}1$$

where:

A_p is the surface area of the pool (m^2)

S_p is the pool perimeter (m)

2.1.2 Shape

The shape of a flame is dictated by the shape and size of the pool diameter and the wind conditions. Shape is important when the solid flame model (explained in more detail below) is used in the calculation of radiative hazards. Usually, a circular cylinder is used to describe a fire plume. However, other geometries, such as conical, parallelpiped, and elongated base cylinder shapes, are commonly accepted [4]. For a cylinder configuration, the height is given by the height of the flame, and the base is taken as the diameter of the pool. The flame is usually assumed to be perpendicular to the pool surface under low wind conditions, and a tilted cylinder when wind speeds are above the critical wind speed (u^*>1) [8]. This threshold is called the non-dimensional wind velocity and it is described in subsection 2.1.3. Figure 3 contains a sketch of the main characteristics of the flame's geometry.

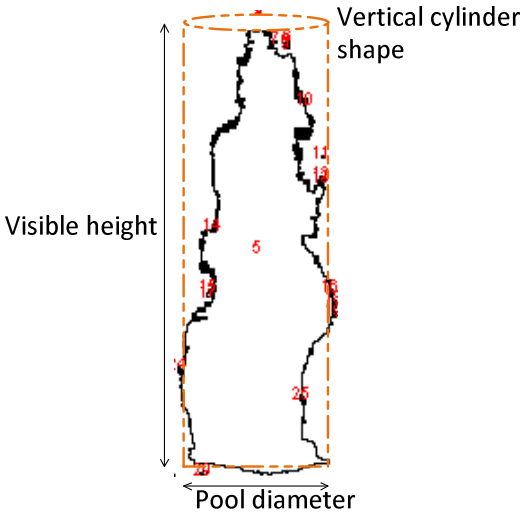

Figure 3. Sketch depicting the main attributes of a flame

2.1.3 Height

Height refers to the length of the flame above the liquid surface. Commonly, the term height is used to describe the vertical distance between the base and the top of the flame and the term length to describe the distance between the highest point of a tilted flame and its base. A number of attempts in the form of correlations have been proposed in the past to describe this parameter and as a result, up to 3 differentiation zones can be found in the literature to characterize a flame height. Most often, a parameter called “mean visible plume length” is used to represent the flame height. The two-plume region includes a lower region characterized by a steady flame, and an upper region characterized by the intermittency of the flame, in which the formation and detachment of eddies is evident [13, 15]. A three-region zone usually encompasses a continuous flame region, an intermittent flame region, and a plume region [16-17] distinguishable by temperature profiles along the axis of the flame. Figure 4 shows the representation of the differentiation zones for the flame height of a pool fire.

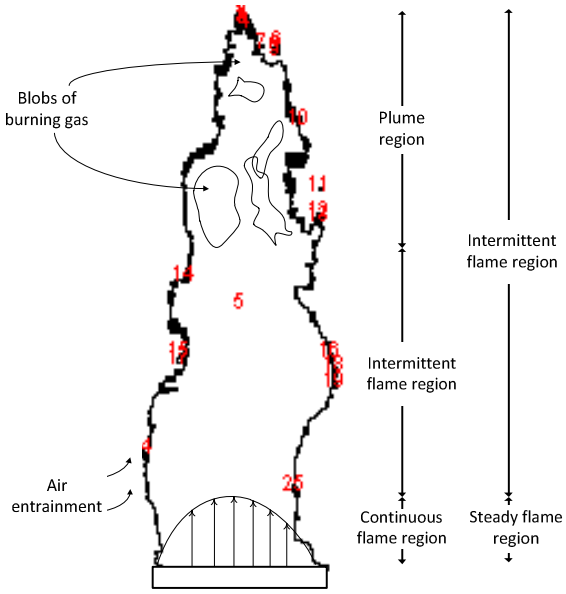

Figure 4. Modified schematic depicting the different zones of the visible flame height [13]

Most correlations proposed for calculation of flame heights are based on experimental data, and in some cases physical implications are included. As discussed by Raj [18], caution must be exercised when using these correlations for the calculation of radiation hazards for large pool fires where smoke production clearly has an influence on the visible flame height. Following is a list of correlations that can be used for the prediction of flame height for pool fires. The intent of this list is not to be comprehensive, but to provide an idea of the different correlations proposed in the literature.

- Thomas correlation [19]: $\frac{H}{D} = 42\left(\frac{\dot{m}''}{\rho_a\sqrt{gD}}\right)^{0.6}$ 2-2
- Modified Thomas correlation [19]: $\frac{H}{D} = 55\left(\frac{\dot{m}''}{\rho_a\sqrt{gD}}\right)^{0.67} u^{*(-0.21)}$ 2-3
- AGA correlation [20]: $\frac{H}{D} = \left(\frac{\dot{m}''}{\rho_a\sqrt{gD}}\right)^{-0.19} u^{*(0.06)}$ 2-4

where:

$$u^* = \frac{u_w}{\left(\frac{g\dot{m}''D}{\rho_a}\right)^{1/3}}$$

$\dot{m}''$ is the mass burning rate (kg/m^2·s)

ρ_a is the air density (kg/m^3)

g is gravity (m/s^2)

D is pool diameter (m)

H is flame height (m)

u^* is the dimensionless wind velocity

u_w is wind speed (m/s)

2.1.4 Tilt

The tilt of a flame describes the angle between the vertical axis and the inclined flame due to high wind speeds. Correlations found in the literature for the description of this parameter include those of Thomas [4], Welker and Sliepcevich [21], and A.G.A [20].

- Thomas: $Cos\theta = 0.86\left[\frac{u_w}{(g\dot{m}''D/\rho_a)^{1/3}}\right]^{-0.25}$ 2-5
- Welker and Sliepcevich $\frac{\tan\theta}{\cos\theta} = 3.3\left[\frac{Du_w}{v}\right]^{-0.07}\left[\frac{u_w^2}{g\cdot D}\right]^{-0.8}\left[\frac{\rho_v}{\rho_a}\right]^{-0.6}$ 2-6
- A.G.A: $Cos\theta = 1$ for $u^* < 1$ 2-7

  $Cos\theta = (1/u^*)^{1/2}$ for $u^* > 1$

where:

v is the air viscosity (m^2/s)

ρ_v is the vapor density of the fuel at its boiling point (kg/m^3)

θ is the angle between the tilted flame and the normal line to the ground

2.1.5 Drag

The drag of a flame refers to the extension that occurs on the base of the flame due to the wind as seen in Figure 5. Drag is seen in the downwind direction and it does not affect the edge of the flame in the upwind direction. Welker and Sliepcevich [21] formulated the following equation for the calculation of the extension of the diameter due to windy environments:

$$\frac{D'}{D} = 2.1Fr^{0.21}(\rho_v/\rho_a)^{0.48} \quad \text{2-8}$$

where:

$Fr = {u_w}^2/gD$

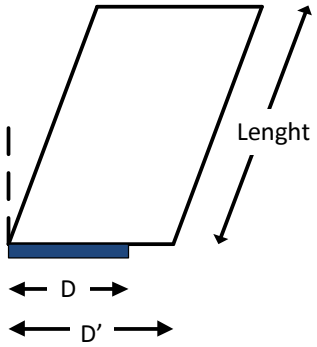

Figure 5. Sketch showing the parameters involved in the calculation of the flame drag

2.2 Pool fire characteristics

The amount of radiant heat received by an object depends on the characteristics of the pool fire, mainly the radiant heat emitted by a fire, which in turn depends on the emissive power of the flame. The emissive power subsequently depends on the flame geometry and the fuel's burning rate.

2.2.1 Burning rates

The rate of fuel evaporation from a pool fire is commonly referred to as its mass burning rate (kg/m^2.s) and its velocity as the linear regression rate (m/s). The description of these parameters relates to the effects arising from a pool fire. Therefore, care needs to be taken when reporting and handling data. Commonly, burning rates are obtained using a semi-empirical correlation such as:

- Zabetakis and Burgess [22] $\dot{m}'' = m_\infty(1 - e^{-k\beta D})$ 2-9

where:

m_∞ is the mass burning rate for large pool diameters (kg/m^2·s)

k is the extinction coefficient of the flame (m^{-1})

β is the mean beam distance (dimensionless)

In 1974, Burgess proposed a variation of this equation based on the limited availability of the empirical parameters. The equation for the calculation of mass burning rates based on the properties of the fuel is:

- Burgess [4] $$\dot{m}'' = \frac{CHc}{\Delta Hv + C_p(T_b - T_a)}$$ 2-10

where:

ΔH_v is the heat of vaporization for the fuel (kJ/kg)

C_p is the heat capacity (J/kg·K)

T_b is the boiling temperature of the fuel (K)

T_a is the ambient temperature (K)

C is equal to 0.001 (kg/m^2·s)

H_c is the heat of combustion (kJ/kg)

The first term of the denominator corresponds to the heat given off by the change in phase and the second one to the sensible heat of the material. For cryogenic liquids, which are usually stored at their boiling points, the second term is null.

Experimentally, burning rates can be reported as a mean property, a maximum value, or a curve that displays its complete behavior with time.

2.2.2 Thermal radiation

To calculate the thermal radiation that reaches an object, parameters such as the radiant power of the flame, size and shape of the flame, and atmospheric transmission need to be known. The correct description of these parameters will have a direct impact on the credibility of the calculated scenario.

Thermal radiation is usually calculated from semi-empirical models, mainly, the solid flame model and the point source model [4, 23]. These models present drawbacks such as uncertainty in the calculation of scenarios different from those validated, since at best the experimental parameters used in the calculation will be extrapolated values [13]. Further, experimentally obtained parameters are only available for specific conditions, and assumptions are usually incorporated in the models for simplicity. Computational Fluid Dynamics (CFD) or field models such as CFX and Fluent have also been used for this type of calculation. However, similar to semi-empirical models, they have only been validated over a specific range and, due to their complexity, may involve extensive computational time. Integral models such as PHAST[1] (Process Hazard Analysis Software Tool) are a good compromise between the simplicity of the semi-empirical models and the complexity of CFD models. However, integral models are still not 100% reliable due to the inadequacy of the predictions resulting from certain fire scenarios.

- Point source model

$$q'' = \eta \dot{m}'' \frac{\Delta Hc}{4\pi X^2} \qquad 2\text{-}11$$

where:

X is the distance between the object and the source

[1] http://www.dnv.com/services/software/products/safeti/safetiqra/phast.asp

η is the fraction of energy radiated from the released combustion energy

The main advantage of this model is the simplicity of the calculation due to the assumption that the emitted radiation originates from a point source of the flame without regard to the shape of the flame. Main drawbacks of this model include the conservative estimates resulting from the assumption that the receiving objects will always receive the maximum amount of energy, regardless of the geometry of the flame or its orientation with respect to the object, and the estimation of the fraction of energy radiated from the heat released from the combustion of the gases. It proposes a reduction of the radiated energy with the inverse of the square distance to the object. This model should be used as a preliminary tool that generates a conservative estimate. Caution should be exerted if used for a facility layout [4].

- Solid flame model

$$q'' = SEP_{act} F_{view} \tau_a \qquad 2\text{-}12$$

where:
τ_a is the atmospheric absorption (dimensionless)
F_{view} is the geometric view factor between the flame and the object
SEP_{act} is the actual Surface Emissive Power emitted by the flame

The τ_a is mainly due to the absorption of the water vapor and CO_2 found in the atmosphere. As reviewed by Mannan [24], a number of correlations are available to correct the radiation data for atmospheric absorption. Frequently, the charts from Hottel and Sarofim [25] are used for the calculation of τ_a. However, it is important to mention that these procedures are an estimate based on a number of assumptions and, thus, have an associated uncertainty [8, 10].

Therefore, the results presented in this work are given without correction for atmospheric absorption.

The geometric view factor accounts for the flame shape, the receiving object orientation, and the distance that separates them. For the vertical cylinder type flame, the maximum view factor is calculated as follows [26]:

$$F_{view} = \sqrt{F_v^2 + F_h^2} \qquad 2\text{-}13$$

where:

F_v is the vertical view factor, and F_h is the horizontal view factor. These individual factors are explained below,

$$\pi F_v = \frac{a}{b}\frac{a^2+b^2+1}{[a^2+(b+1)^2]^{1/2}[a^2+(b-1)^2]^{1/2}} tan^{-1}\left[\frac{a^2+(b+1)^2}{a^2+(b-1)^2}\right]^{1/2}\left(\frac{b-1}{b+1}\right)^{1/2} + \frac{1}{b}tan^{-1}\left(\frac{a}{b^2-1}\right) - \frac{a}{b}tan^{-1}\left(\frac{b-1}{b+1}\right)^{1/2} \qquad 2\text{-}14$$

$$\pi F_h = tan^{-1}\left(\frac{b+1}{b-1}\right)^{1/2} - \frac{a^2+b^2-1}{[a^2+(b+1)^2]^{1/2}[a^2+(b-1)^2]^{1/2}} * tan^{-1}\left[\frac{a^2+(b+1)^2}{a^2+(b-1)^2}\right]^{1/2} * \left(\frac{b-1}{b+1}\right)^{1/2} + \frac{1}{b}tan^{-1}\left(\frac{a}{b^2-1}\right) - \frac{a}{b} \qquad 2\text{-}15$$

a corresponds to the ratio between the flame height (or length) and the flame radius and b corresponds to the ratio between the observer distance and the flame radius. These parameters can be observed in Figure 6.

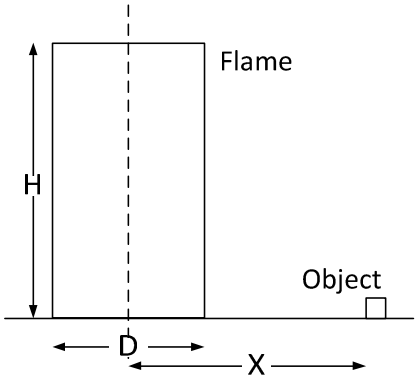

Figure 6. Sketch depicting the parameters used to describe the view factor. This geometric factor corresponds to a flame assumed to be a vertical cylinder

This commonly used model predicts the radiative heat emitted by a flame that reaches an object at a particular distance, accounting for the attenuation of the energy due to atmospheric absorption and the orientation and distance of the object to that of the flame. The main drawback is the assumption of a uniform flame that emits energy from its entire visible surface without regard to the invisible burning gases on the inside and upper regions of the flame. Usually, the flame shape is determined by incorporating Thomas' correlation for the calculation of the flame height (usually a cylinder). Despite these limitations, this semi-empirical model is still widely used and is an improvement from point source model estimations.

2.2.3 Surface emissive power

The Surface Emissive Power (SEP) of a flame refers to the rate of heat released from the combustion sustained in the fire, per the idealized surface inferred average area of the flame. This emissive power is dependent on the geometry of the fire and the type of fuel. This parameter can be predicted by correlations found in the literature [4] or from experimental data [7, 11]. A number of approaches have described the flame SEP in terms of the emissivity

of the different zones of the flame in regards to the height and the emissivity of dominant combustion products such as CO_2, H_2O, and soot particles. Mudan's approach assumes a uniform SEP over the entire surface of the flame and as a function of the flame area, the heat of combustion, a fraction of energy radiated, and a fraction for the reduction of the energy radiated due to soot shielding effect [4]. Raj's approach [13] includes a constant emissive power zone and a variant emissive power zone with the height of the region above the constant SEP region.

The SEP calculated indirectly from data collected during the execution of experiments involves either the wide-angle radiometer (WAR) or narrow-angle radiometer (NAR) data, or the spectral data of the fire. The former approach involves the solid flame model and requires the description of the shape of the flame and the correction for the atmospheric absorption when WARs are employed. When NARs are employed, the spot SEP of the flame is directly obtained for each spot of the flame where the radiometer was aimed, yet, a correction for atmospheric absorption is still required. The latter spectral data method requires the measurement of the emission spectrum of the flames to calculate the emissive power of the fire [11].

2.3 Previous relevant research

2.3.1 Mass burning rates

Research on mass burning rates, flame geometry, and thermal characteristics of hydrocarbon fires have been ongoing since the 70's. Blinov and Khudyannov [27] published a large number of data on the burning of liquids in small diameter open trays. Hottel [28] analyzed Blinov's work, resulting in the formulation of a relationship between mass burning rates, pool diameter and the energy input to the liquid pool. Zabetakis and Burgess [29] further examined

Hottel's work to validate his result with liquid hydrogen and the formulation of a correlation for the prediction of mass burning rates based on empirical parameters. In 1983, Babrauskas [22] focused on larger scale experiments and tabulated values for the empirical parameters used in Burgess' equation. Subsequent efforts focused on the study of mass burning rates of fuels such as non-boiling hydrocarbons, alcohols, and cryogenic liquids of laboratory and intermediate scale [30-33].

2.3.2 Pool fires

Research efforts have also targeted the study of the flame structure, radiation models, and combustion characteristics of pool fires [19, 21]. Radiative heat feedback has been addressed for cryogenic and non-boiling liquids through a number of experiments of a diverse scale [34-35]. Further experimental studies were performed in increasing size on land and on water to study the thermal radiation emitted by a pool fire to the surroundings [8, 12]. Table 1 contains related information for spills on land.

Table 1. Summary of some experimental studies of pool fires on land [8, 10, 34].* These experiments were performed in a square pit

Study reference	Pool diameter (m)
US Bureau of Mines	0.38, 3x3*, 6x6*
AGA	1.8, 6.1
Maplin Sands	20
Montoir	35

3. EXPERIMENTAL PROCEDURES AND METHODOLOGY

A series of three small-scale experiments was performed outdoors during two days at the Brayton Firefighter Training Field in December 2009 to simulate a LNG pool fire on land. The experiments were carried out to measure a number of variables such as temperature, heat flux, liquid level, evaporation rates, radiative heat, and atmospheric conditions, and to study the mass burning rates. This data was gathered by sensors positioned both inside and outside the containment area. Figure 7 shows a schematic containing the set up used inside the pit area.

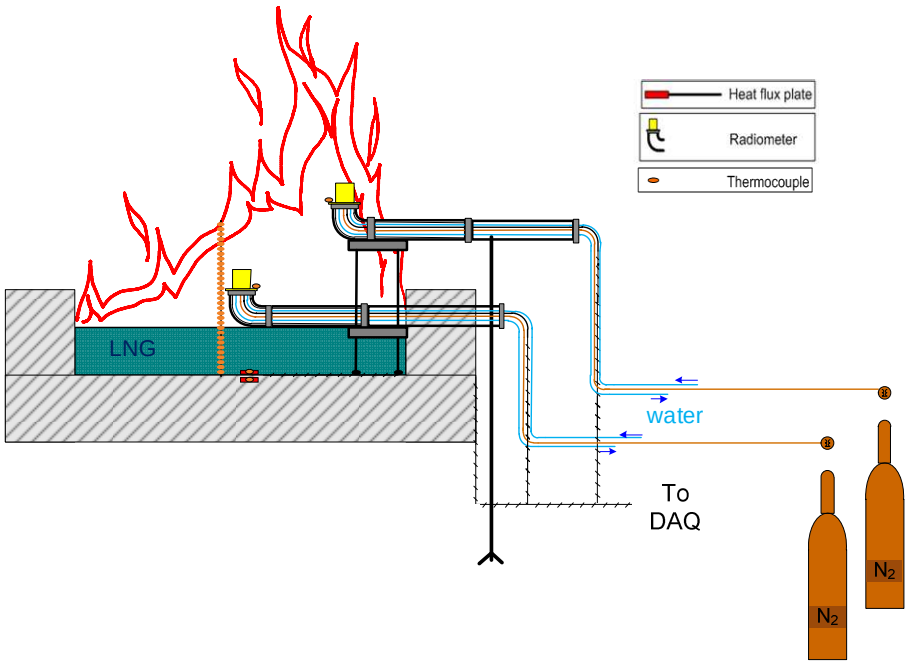

Figure 7. Schematic of the experimental set up inside the pit

3.1 Concrete pit

The tests were performed in a small concrete pit fabricated at this facility. The pit, 1.0 m X 1.0 m X 0.2 m (40 in X 40 in X 9 in) was made out of cellulose concrete, 0.254 m (10 in) thickness. The advantages of cellulose concrete

include its light weight and thermal insulation properties. Figure 8 displays a photograph of the pit used. The dimensions of this pit were chosen so the prevailing heat transfer was that of the radiation, as found in Hottel's work [28]. According to Hottel, the dominant heat of transference is convection for pool fires smaller than 0.2 m of diameter and radiation for those pool's diameters larger than 0.2 m.

Figure 8. Photograph of the concrete pit

3.2 Facilities

The facility is located at the Texas Engineering Extension Services (TEEX), a Division of the Texas A&M University System in College Station, Texas. Figure 9 shows an aerial view of the LNG facility within the Brayton Fire Training Field where the test was conducted. The area surrounding the pits is made of high weight concrete and is sloped toward the pits to avoid spreading in case of an LNG spill. Figure 9 also shows the position where the mobile pit was

located. This site was chosen based on safety considerations to prevent LNG escaping from the site.

Figure 9. Aerial view of Brayton Fire Training Field. The arrow indicates the position of the pit

3.3 Instrumentation and equipment

- Thermocouples

Measurements of the liquid and gas layer temperatures were made by means of k-type thermocouples, (Omega Engineering Inc) spaced out on a metal bar inside the pit. In addition, two thermocouples attached to the radiometers were used to calculate the thermal radiation input to the pool. This type of thermocouple measures temperatures in the range of –270 to 1372℃ and has a ± 1.1℃ accuracy. Features such as ceramic fiber insu lated cables, shielded from abrasion by Inconel 600 rough braiding, with Inconel collars, and ceramic protected bead leads were incorporated in the thermocouples to assure their integrity. Temperature measurements were later converted to LNG

evaporation rates. Figure 10 shows the arrangement used for the positioning of the thermocouples on day 2.

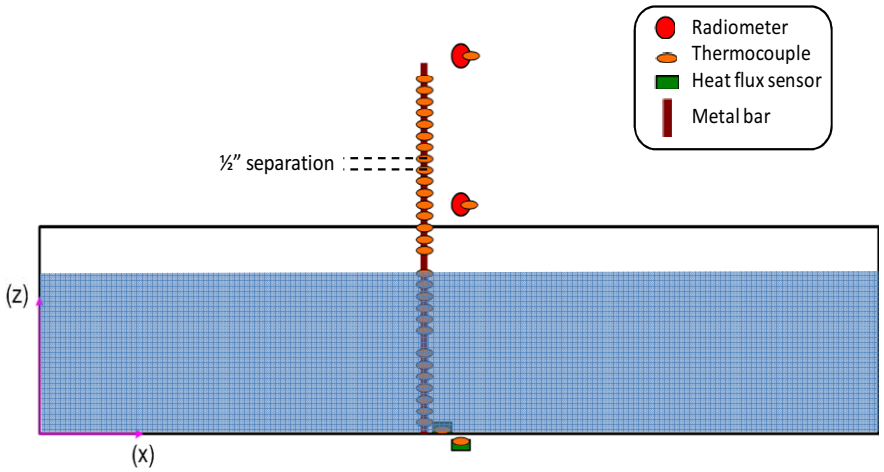

Figure 10. Schematic showing the arrangement of the thermocouples inside the pit area

- Heat flux transducer/ Infrared radiometers

Two models of radiometers from Medtherm Corporation were used with different objectives in mind. Inside the fire, two water-cooled, nitrogen-purged radiometers were located at two different elevations from the liquid surface to measure the radiative heat transfer from the flame to the liquid pool (Figure 11).

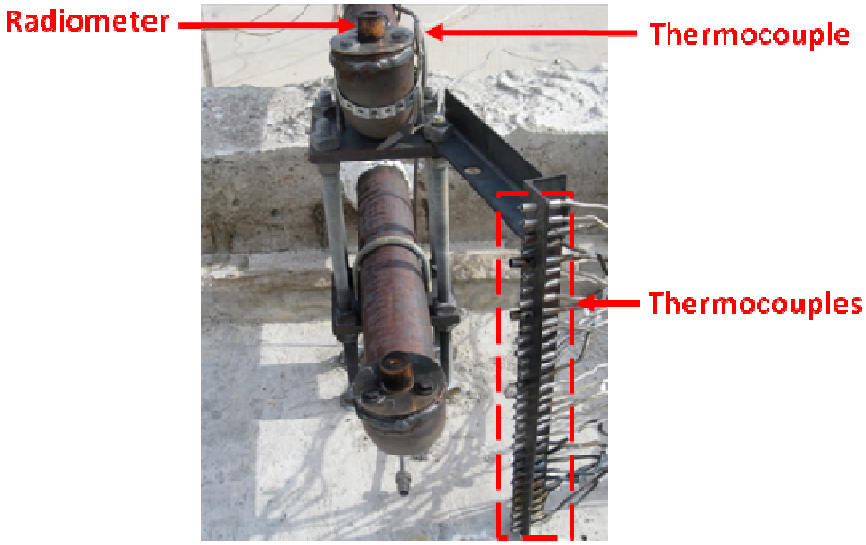

Figure 11. Picture displaying the arrangement and orientation (upward) of the radiometers inside the pit

Sapphire windows were used to eliminate the convective heat from the heat flux measurements and exclusively obtain measurements of radiative heat. Water cooling was used to avoid condensation of water on the window and to maintain a constant heat sink temperature reading on the sensor when immersed in a flame. Nitrogen purging was used to reduce the deposition of soot particles on the window of the sensor.

The type of sensor used was a Schimidt-Boelter gage. The operating principles are based on the difference in temperature between the sensor (heat sink) and the source. This sensor has the advantage of a higher sensitivity and a lower response time when compared to Gardon gages [36].

The expected uncertainty for this type of sensor is $\pm$3%, according to calibration specification from the vendor. Figure 12 shows a sample picture of the radiometers used and a cross section drawing to display its features.

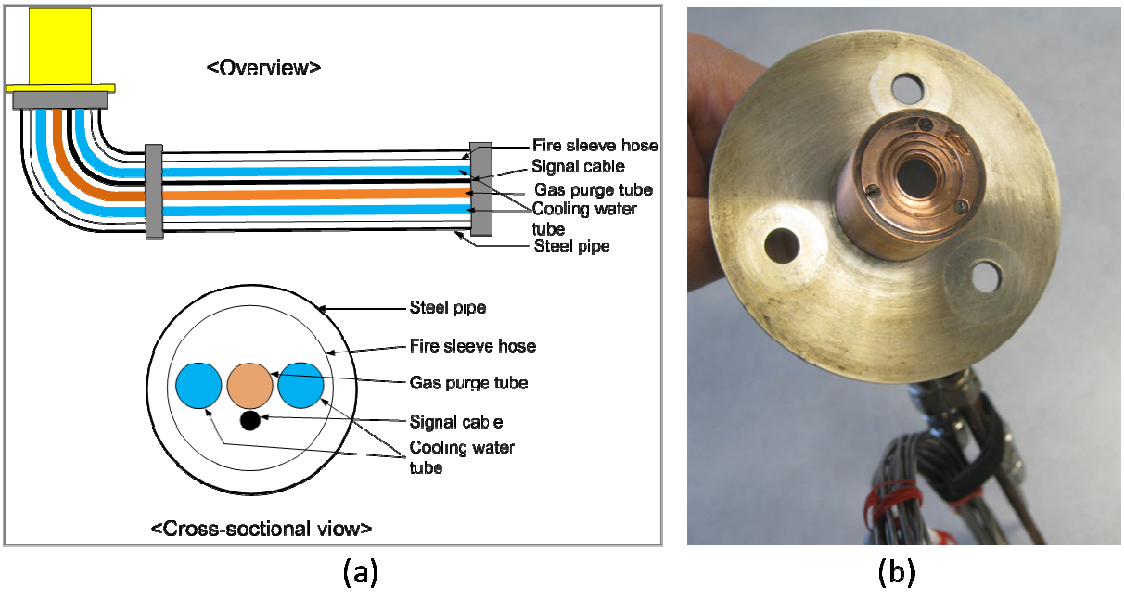

Figure 12. Radiometer view. (a) corresponds to a cross section view and (b) corresponds to a photograph of the sensor

Outside the pit, two radiometers were positioned in the downwind direction, 0.9 m (3 ft) from the ground, mounted on a tripod to measure the heat flux from the fire to the surroundings, and to obtain the average surface emissive power of the flame as shown in Figure 13. Similarly, according to calibration specifications from the vendor, the uncertainty for the response is ±3%, and the view angle of the window was limited to 150°. These radiometers did not require a water-cooling system, because exposure to temperatures higher than 400℉ (according to vendor specifications) was limited.

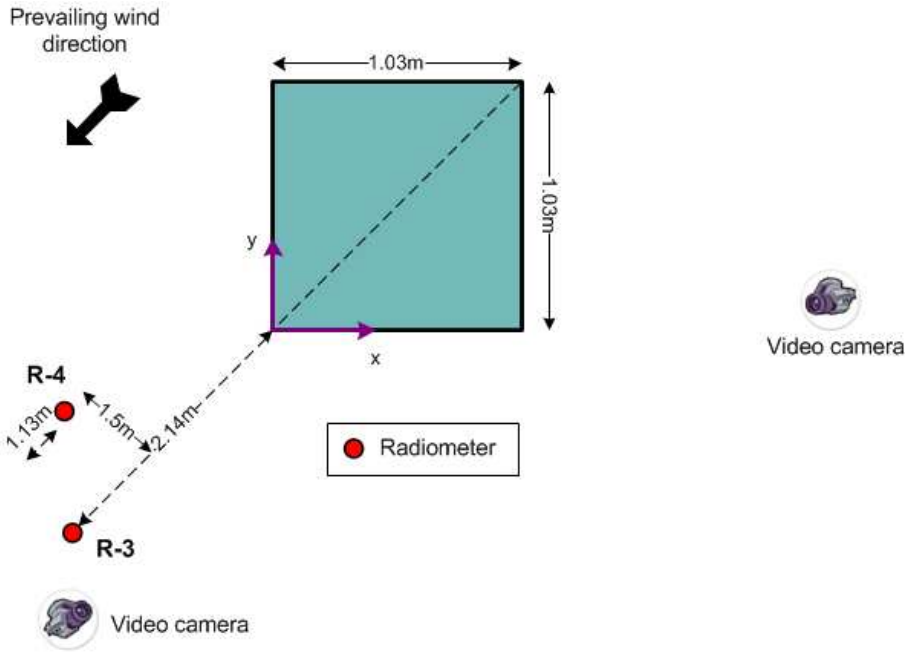

Figure 13. Layout of radiometers outside the pit

- Heat flux sensors

In order to measure heat fluxes between the concrete floor and the liquid fuel, two heat flux sensors with integral k-type thermocouples were located inside the pit. One was positioned on the interface of the concrete-LNG at the bottom of the pool and the second one was embedded 1.3 cm (1/2 in) under the concrete surface. Associated thermocouples measured the temperature at the bottom of the pool. The sensitivity of the sensor is 0.90-0.97 $\mu V/W/m^2$ and the response time is 0.60 seconds.

- Weather stations

Ambient temperature, wind direction and speed, humidity and atmospheric pressure were measured with a weather station mounted on a tripod, 2m above the ground. These parameters were recorded every 60 seconds.

- Differential Pressure Transmitter

The change in LNG level in the pit was measured by means of a differential pressure transducer, which uses as a reference point the pressure created by a relatively constant flow of a nitrogen source located at a fixed position and measured by one end of the transmitter. This reference point is used to compare the hydrostatic pressure created by the liquid level recorded by the other end of the transmitter located at the bottom of the pit. The difference between these two variables is constantly being recorded and converted to an electrical signal that relates the change in liquid level with the associated difference in pressures.

- Data collection equipment

A data acquisition (DAQ) system was used as an interface for the equipment used in the field to collect the data during the experiment. The only exceptions to this are the weather stations, which have a built-in system. This interface was then connected to a computer located in a remote position to store the gathered data. The system, from IOTECH, is an Ethernet-based system, capable of handling a large number of sensors simultaneously by the use of various modules for signal conditioning.

3.4 Procedure

The discharge of continuous LNG was carried out with a low flow rate (around 50 GPM for test 1 and 2, and less than 20 GPM for test 3) to avoid LNG splashing outside the pit. The purpose of the pool fire tests was to obtain a steady (low-boiling) liquid pool with low droplet turbulence by using delayed ignition. After the pool filled to the desired point, it was left to vaporize before being ignited. This part of the test lasted for a period of about five minutes. After

that, the pool was ignited on an edge and the flame spread rapidly across the pool surface. Once ignited, the data were collected until the flame was extinguished by fuel consumption for tests 1 and 2.

4. RESULTS AND DISCUSSION

Although the discussion of the results is based on the entire set of experiments performed, the plots displayed in this document correspond only to those of test 2 to avoid showing multiple plots of similar trends. In addition, to reduce the noise in the data collected, to observe the trends clearly, and to study the effect of the parameters measured, moving averages were used to present the experimental data.

4.1 Experiment details

Table 2 contains a summary of the atmospheric conditions as well as other relevant information measured during the experiment at the field site.

Table 2. Summary of experiment details

Category	Parameter	Test 1	Test 2	Test 3
Atmospheric conditions	Temperature [°C]	9.01 ± 0.18	10.74 ± 0.75	7.20 ± 0.12
	Average wind speed [m/s]	2.90 ± 0.62	1.28 ± 0.55	0.5 ± 0.35
	Wind direction	S & SSE	SE & ESE	S & SSW
	Relative humidity [%]	45.53 ± 0.68	61.97 ± 4.11	55.16 ± 0.93
	Solar radiation [W/m^2]	60.2 ± 10.85	0	0

Table 2. Continued

Category	Parameter	Test 1	Test 2	Test 3
LNG details	Methane composition [%]		~ 99.87	~ 99.87
	Initial liquid level [m]	0.10	0.16	0.17

As mentioned above, the geometry of the flame is affected by wind speed; however, the low wind speeds under which tests 2 and 3 were performed (less than 2 m/s) had only a small influence on the flame properties. Tests 2 and 3 were started in the late afternoon and continued after sundown. This explains the absence of recorded solar radiation. The LNG compositions in Table 2 show that the fuel was mainly one component and, as such, the behavior was mainly that of methane. This translated into a faster stabilization of the liquid pool and a clearer burning since soot production is related to a hydrocarbons' molecular weight. The initial liquid level before ignition varied according to the volume of the LNG spilled in the dike, the different spill periods, and the heat transfer that resulted in a variable volume of LNG vaporized during the free evaporation periods.

4.2 Geometry of the flame

The visible height, bend angle, and apparent surface area of the flame were determined by the analysis of the recordings obtained during the experiment from the video cameras positioned in two fixed locations, as seen in Figure 13.

4.2.1 Flame height/length

The flame characteristics were obtained by two different methods: analysis of the experimental data and semi-empirical calculations from correlations in the literature. The first method involved the conversion of the video file into still photographs taken at 1 second intervals and further analysis by means of the image processing software ImageJ[1] (developed at the National Institutes of Health), which included a number of steps. A subroutine was developed to perform the following steps in a batch mode: a) uploading of a specific photo, b) modification of the format and the brightness, c) definition of a threshold, d) measurements of the flame in pixel units, and e) storage of results. Further analysis included setting a reference scale and converting the pixel data into length units.

Figure 14 depicts a typical photograph gathered during the second day of testing of the LNG pool fire corresponding to test 3. As mentioned before, this fire corresponds to a pure methane burning period at steady-state. The observed flame was of a bright yellow coloration, with low soot formation, and had a vertical cylinder like shape during low wind conditions. Three subtle regimens were distinguished from the observations and the analysis of the recordings:

- The first regimen corresponds to the spreading of the fire upon ignition, which was almost instantaneous (< 3 seconds).
- The second regimen consists of a stable period where the flame height seemed to remain constant, and
- The final regimen includes a decay period where the flame self-extinguished in tests 1 and 2. This third regimen was not achieved in the last test since the flame was extinguished when approximately 2 inches of liquid were remaining in the pit.

[1] http://rsbweb.nih.gov/ij/

Figure 14. Typical photograph of the LNG pool fire corresponding to test 3 during the steady-state burning period

Figure 15 shows a sample view of an analyzed file, containing the visible flame height (purple line), the visible flame length (blue line), the tilt angle (ɵ), and the projected surface area (yellow-shaded area). The measurements of the flame, i.e., height, length, and tilt angle, were determined according to the largest surface area found by the program, which corresponded to the flame attached to the pool surface without regard to the flame plumes that are no longer attached to the main flame.

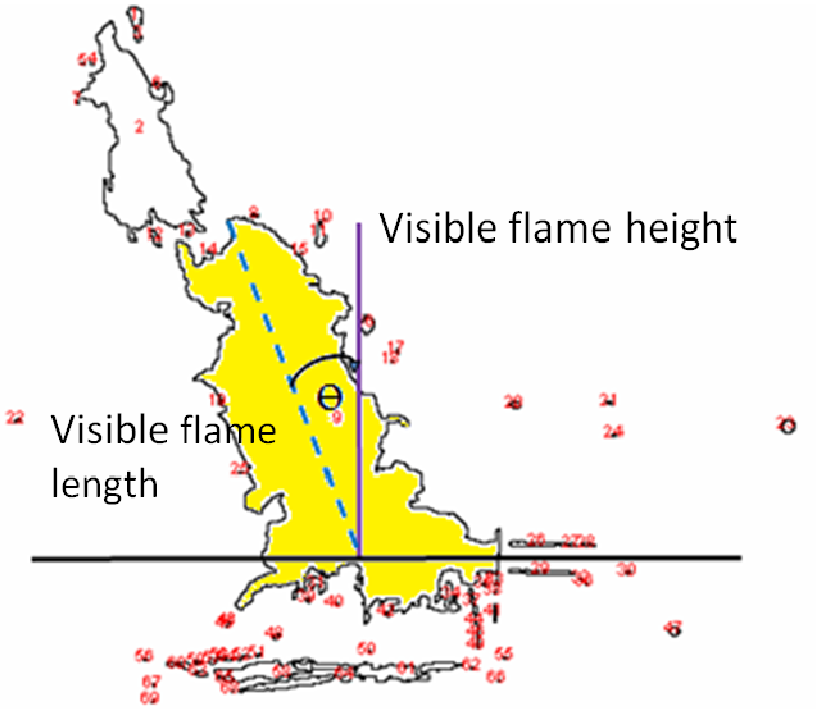

Figure 15. Distinction between visible flame height and visible flame length

Figure 16 shows the results for the visible flame height for both cameras for test 2 with respect to burning time. Similar results were obtained for test 3. Data were not available for test 1 due to changes in the camera settings during the recording time.

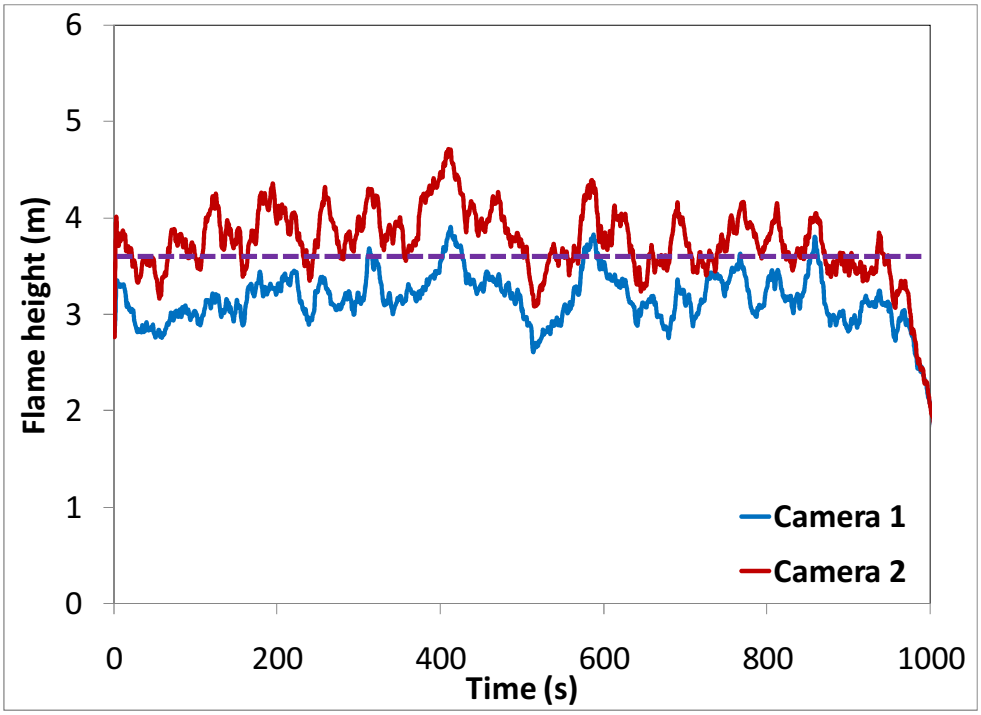

Figure 16. Visible flame height variation. Obtained from the camera recordings

The data displayed in Figure 16 show that the data obtained from camera 1 have good agreement with those obtained from camera 2 and an average of the measured heights seems to provide a representative value of the observed flame height. The transient periods at the beginning of the fire and during the decay of the flame were less than 5 seconds. This was due to the thermodynamic steady-state achieved by the liquid pool prior to ignition with its surroundings. Similarly, the visible flame length due to the effect of the wind on the plume was also calculated and it is shown in Figure 17.

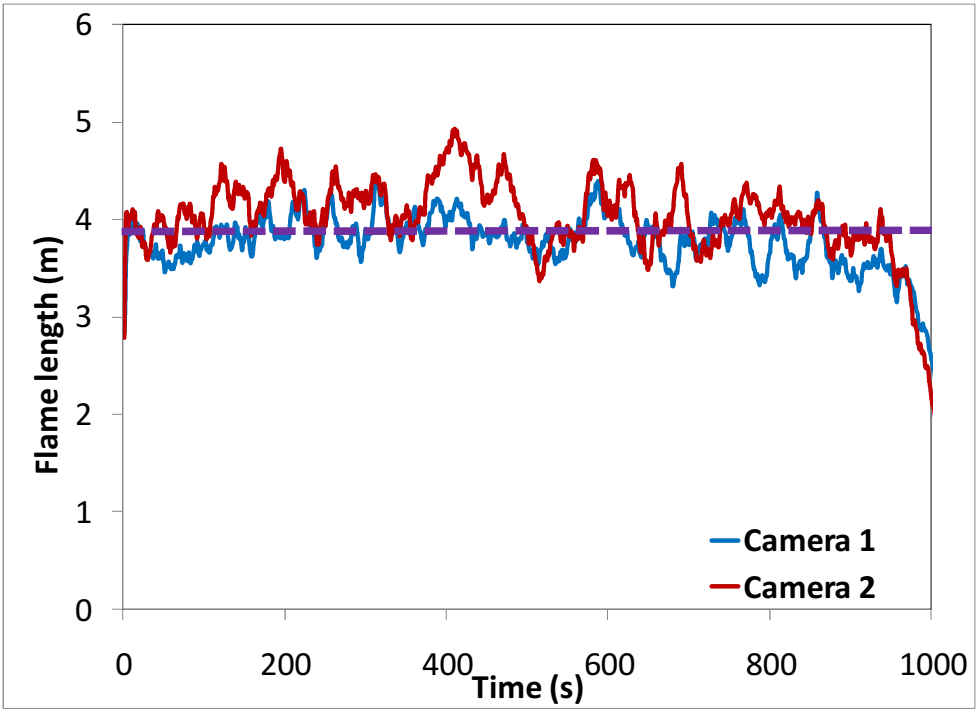

Figure 17. Visible flame length variation. Obtained from the camera recordings

The fluctuations observed in Figure 16 and Figure 17 correspond to a common feature observed in large pool fires. The influence of the wind speed on the variation of the visible flame height is often referred to as the pulsation of the flame and it is characterized by the formation of eddies that evolve from the bottom of the flame, travel through the flame, and finally detach from the top. However, as can be seen in Table 1, the wind speeds experienced during the test were quite low, and the difference between flame heights and the flame lengths is insignificant as reported in Table 3. It can be seen that the ratio of the flame length to flame diameter was approximately 4.

4.2.2 Tilt of the flame

Another characteristic measured during the series of tests includes the angle that the flame is tilted in relation to the vertical axis. The procedure used for its calculation follows that used for the flame height determination and the results are shown in Table 3. As expected, the angle and the flame length are directly dependent on the wind speed. Even though the flame characteristics were not obtained for test 1, from observations, recordings, and pictures, the tilt of the flame appeared to be the shortest one compared to the other experiments. As expected, this corresponded to the largest wind speed recorded.

4.2.3 Projected surface area of the flame

The projected surface area was determined following the procedure described above and is shown in Table 3. It is important to highlight that this surface area does not represent the true area of the flame, since it only describes the surface area in a 2-dimensional view as it was captured by a camera at a fixed position in a fixed time period. This parameter can be used to predict the surface emissive power as mentioned in subsection 2.2.3.

Table 3. Average visible flame plume height, length, bent angle, and projected surface area

Parameter	Test 2	Test 3
Vertical flame [m]	3.4 $\pm$ 0.6	4.0 $\pm$ 0.6
Tilted flame [m]	3.9 $\pm$ 0.6	4.3 $\pm$ 0.6
Tilt angle [degrees]	24.0 $\pm$ 8.4	13.5 $\pm$ 7.3

Table 3. Continued

Parameter	Test 2	Test 3
Projected surface area [m^2]	5.8 $\pm$ 1.1	5.7 $\pm$ 0.8

The values reported in Table 3 correspond to the averages with the respective standard uncertainty.

4.2.4 Comparison

A comparison of the flame height obtained from camera records was done by calculating the empirical values obtained with the equations described in subsection 2.1.3 as seen in Table 4. In addition, the experimental values obtained in this work for flame tilt were also compared to the predicted values that originated from the equations described in subsection 2.1.4. These results are shown in Table 5.

Table 4. Summary of the average visible flame heights calculated with semi-empirical correlations. For comparison purposes, the experimental values are displayed in the last two rows of this table

Correlation	Test 2 [m]	Test 3 [m]
Thomas	3.35	3.47
Thomas modified	3.05	3.47
AGA	2.27	2.25
Visible flame height	3.4 $\pm$ 0.6	4.0 $\pm$ 0.6
Visible flame length	3.9 $\pm$ 0.6	4.3 $\pm$ 0.6

Table 4 lists the results of the flame height calculated with some correlations and the average flame height obtained with the data gathered from the recording frames. Thomas' correlation for still conditions seems to have a good predictive power when compared to AGA. However, when wind speeds are above 1 m/s, the modified Thomas correlation seems to lose its accuracy for this scale.

Table 5. Summary of the flame tilt calculated with semi-empirical correlations. The observed values for this work are displayed in the last row of this table

Correlation	Test 2 [degrees]	Test 3 [degrees]
A.G.A	36.23	0.00
Thomas	40.12	14.26
Welker and Sliepcevich	52.14	30.94
Observed angle	24.0 $\pm$ 8.4	13.5 $\pm$ 7.3

Table 5 shows that the Welker and Sliepcevich correlation overpredicts the tilt angle of the flame for low wind conditions like the ones encountered during this test set. Similarly, the Thomas correlation also gave slightly higher results than the observed tilt angles. The A.G.A correlation gave tilt angles equal to zero because according to the equation, for wind velocities below 1 m/s, the impact of the wind on the flame can be approximated as negligible and a straight flame can be assumed. Overall, it seems that the Thomas correlation gives a good, rough estimate that is very simple to obtain and can be regarded as a good approximation.

4.3 Mass burning rates

Mass burning rates were obtained by means of two straightforward methodologies, which involved the measured temperature profile and the liquid level of the pool. The values obtained from all the experiments performed along with their respective standard deviation are reported according to the guidelines expressing the uncertainty by Taylor [37].

4.3.1 Temperature profile

The elapsed time (ΔT) required for the liquid level of the pool to pass from one thermocouple to the next one located right below it was used to calculate the mass burning rate. This was accomplished by knowing the exact location of each thermocouple in the pool and using the LNG boiling temperature of -156 ℃ as a reference point. In addition, a liquid density of 425 kg/m^3 was used for the calculation. The sudden change in the temperature reading indicated that the liquid had vaporized. This behavior can be seen in Figure 18.

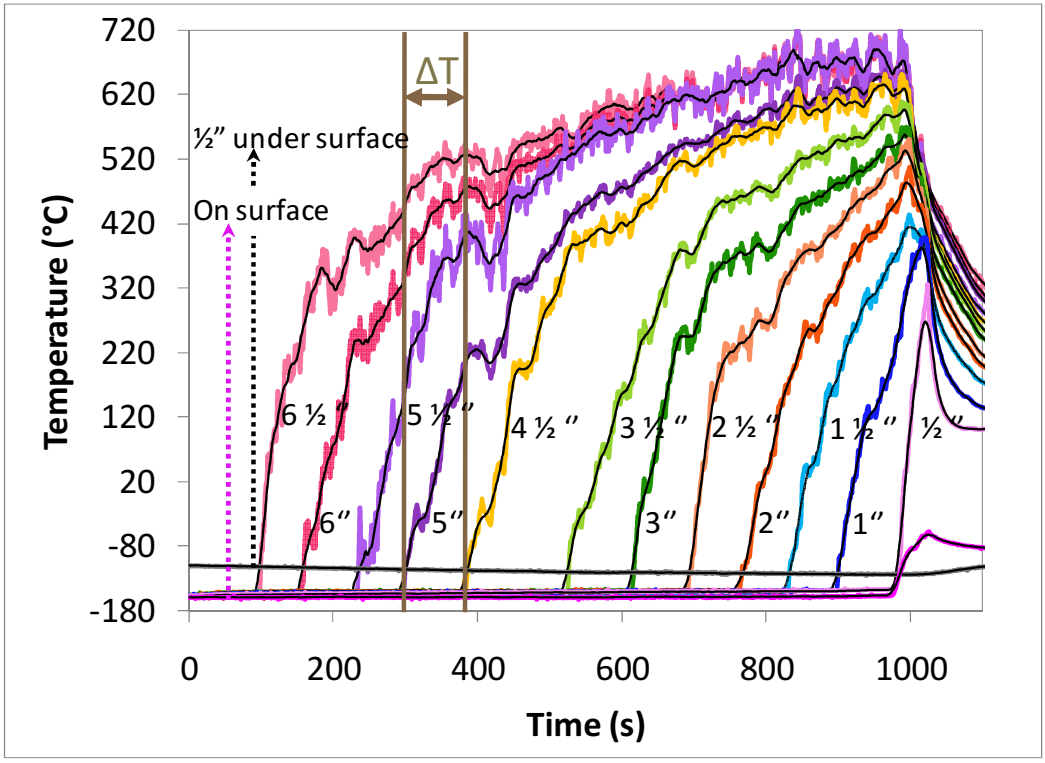

Figure 18. Temperature profile. The vertical position (inches) of the thermocouples increased from right to left as indicated by the numbers in the plot

Table 6 contains the average values for LNG mass burning rates obtained with this method. As can be seen from Figure 18, the mass burning rate was fairly constant during the entire burning period.

Table 6. Summary of the LNG mass burning rates by different methods. Mass burning rates are given in $kg/m^2 \cdot s$

Experiment / Method	1	2	3
A	0.062 ± 0.011	0.075 ± 0.010	0.077 ± 0.014
B	0.05171 ± 9E-05	0.06027 ± 3E-05	0.06466 ± 3E-05
C	0.07 ± 0.12	0.07 ± 0.04	0.07 ± 0.03

4.3.2 LNG level

This method involved the liquid level data obtained from the differential pressure transducer as seen in Figure 19. A straight line was the best fit for the data according to the calculated values for R square (see Appendix). The slope of the line was the average regression velocity. This parameter was then converted to a mass evaporation rate using the density value mentioned above, and the results are displayed in Table 6. The standard deviations reported for method B were obtained from the uncertainties corresponding to the 95% confidence interval of the slope of the line.

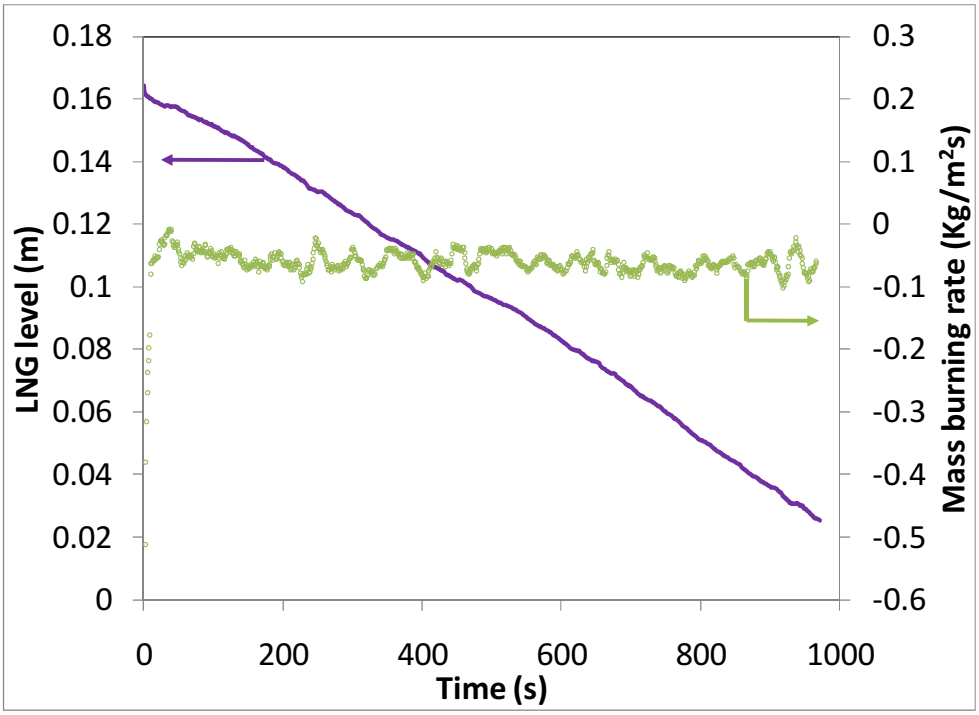

Figure 19. LNG level profile and mass burning rate behavior

In addition, we obtained the mass burning rate curve displaying the typical behavior of an evaporating pool in a steady state. This method, referred to as method C, was used for a more precise validation of method B, to obtain

the instantaneous behavior of the mass burning rate with time, and to observe the transient states at the beginning and the terminal stages of the fire. As can be seen in Figure 19, the free evaporation period prior to ignition brought the pool to a thermodynamic stable state and therefore a rather short transient state was present at the beginning of the burning period. The average values for this parameter are also shown in Table 6.

The comparison of the values obtained with each methodology gave consistent results for all three experiments. Moreover, the evaluation of the values obtained with each different method for individual tests are in agreement, which validates their use for the determination of mass burning rates.

4.3.3 Comparison

To validate the data obtained from the series of tests performed, a comparison was carried out with both values found in the literature and the values predicted from the semi-empirical correlations generated based on previous experiments.

4.3.3.1 Literature

The values obtained through this experimental research were compared with experimental values found in the literature. These values correspond to data from LNG fire experiments on land performed in the past. Data from Babrauskas [22], who compiled data from different sources, is shown in Table 7. It is important to highlight that the comparison is done to show that the values measured in this work are within the same order of magnitude with those obtained in previous studies of pool fires and burning rates. It is impossible to

expect exact reproducibility of the data since the experiments were performed outdoors, and the external conditions could not be controlled nor reproduced.

Table 7. Comparison of mass burning rates with values in the literature. * The mass burning rate was calculated from the reported regression rate and a density value of 425 kg/m^3

Diameter (m)	**Mass burning rate (kg/m^2·s)**	**Reference**
0.75	0.042	[22]
1.52	0.047	
1.8	0.022	
1.8*	0.064	[8]

Although the experimental values obtained in this work seem to fall on the higher side of the spectrum of reported mass burning rates, as mentioned above, the order of magnitude of these results is in agreement, so the values can be regarded as reliable due to their repeatability through the 3 experiments performed.

4.3.3.2 Correlations

The correlations described in subsection 2.2.1 were used to predict the values of LNG mass burning rates. The results along with the assumptions included in the calculations are shown in Table 8.

Table 8. Comparison of mass burning rates with values obtained from correlations

Correlation	Mass burning rate (kg/m^2·s)	Notes
Zabetakis and Burgess	0.056	m_∞ was taken as 0.078 ± 0.018 kg/m^2.s and $k\beta$ equal to 1.1 ± 0.8 m^{-1}
Burgess	0.098	Hc was taken as 50 MJ/kg and ΔHv equal to 510 kJ/kg

The Zabetakis and Burgess correlation is based on empirical data and as such, it includes a number of assumptions that need to be met to improve the prediction capacity of the correlation. Some of the conditions of the test were in conformity, such as the steady burning requirement and the freeboard height. However, we can attribute the difference between the experimental values and the predicted one to the wind speeds experienced that were low, but can still alter the prediction power of the correlation since it has been validated for a wind-free environment. On the other hand, the Burgess correlation, which is based on the thermodynamic properties of the fuel, gave weaker predictions for this type of scale. Therefore, if the parameters are tabulated for the Zabetakis and Burgess correlation, the results for a small-scale scenario can be regarded as reliable, but with caution.

4.4 Heat flux transfer

The analysis of the heat transfer was done using the data from the heat flux sensors, the radiometers, and the differential level transducer. To do this, the experiment was divided into individual stages identified as filling, evaporation, and burning periods.

4.4.1 Differential level transducer

Three different stages were clearly distinguished through the analysis of the data gathered by the differential transducer. Each of these regions corresponds to a type of operation: filling (zone 1), evaporation (zone 2), or burning (zone 3) as seen in Figure 20.

The red line corresponds to the zero given by the sensor prior to the experiment. The region corresponding to the filling of the dike (shown in green) was the shortest one for all experiments, with an approximate time interval of 250 seconds for test 2. The time used for filling the dike for test 1 was under 250 seconds and around twice the time of test 1 for test 3. The differences in the filling times correspond, as mentioned before, to the level of the liquid in the pit and the differences in the flow rate.

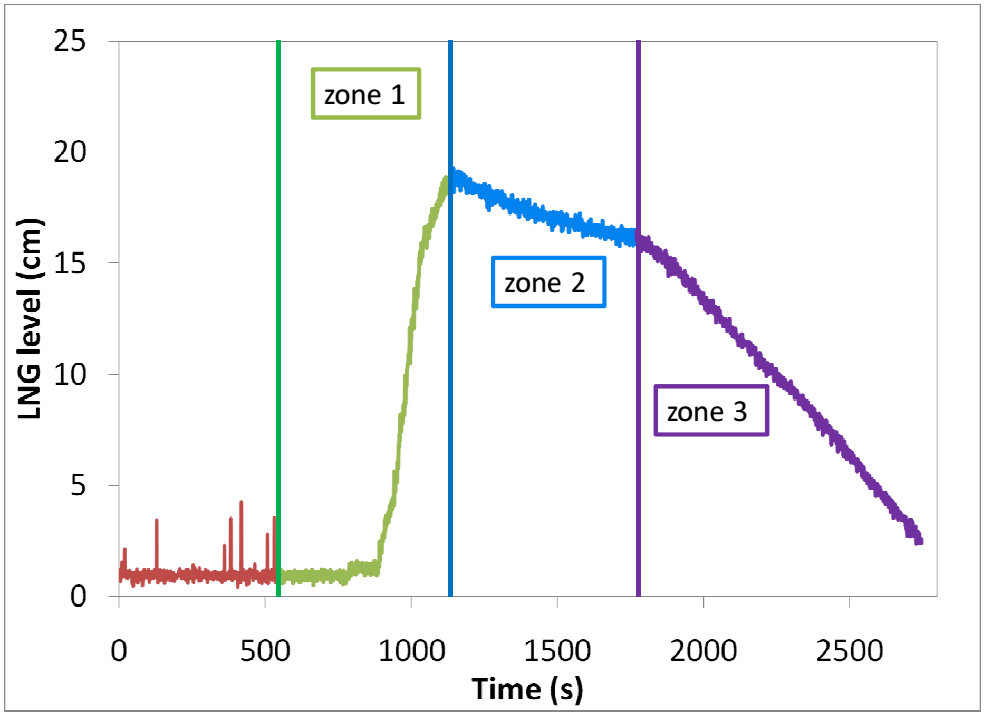

Figure 20. LNG level profile and distinguished stages of operation

Following this, the liquid pool was left to boil off until a stable state was achieved with the surroundings (zone 2). The cutoff of this zone was a subjective assessment of the change in the heat transfer and the temperature of the pool recorded at the time of the experiment. This was determined at the experimentation site according to the variation of the data records. The stabilization of the temperature basically indicated that the evaporation of natural gas at the specific position of the thermocouple recording the temperature was very low and that the liquid layer was at its boiling temperature. This stabilization was the main parameter that determined when the heat flux transfer from the concrete to the liquid pool declined enough in magnitude so it will not be a dominant force for the evaporation of the LNG once the pool was ignited. The evaporation period was about 600 seconds for all tests. The slope of the fitted line corresponds to the vaporization velocity due to the heat transfer from the concrete and the air movement to the liquid pool.

Finally, zone 3 corresponds to the burning period. It was found that for test 2, the burning period was close to 1000 seconds with a vaporization velocity corresponding to the heat transfer mainly by the heat radiated back to the pool from the flame. A factor of roughly 3 indicates the difference in the vaporization velocity between zone 3 and zone 2. The value of this parameter showed that the vaporization rate of the fuel was remarkably higher compared to that when there was no fire. Furthermore, this result indicated that heat transfer due to other means could be neglected when compared to the radiative heat transfer from the fire.

4.4.2 Heat flux sensors

As mentioned above, two heat flux sensors were used to measure the conductive heat input to the pool by the concrete as shown in Figure 21a.

Initially, during the filling operation, the sensor's reading was very low due to the continuous cool down of the discharge pipe and the surroundings. The subsequent increase seen in the heat input from the concrete surface to the pool is due to the beginning stage of the cooling of the concrete pit. This implied that the environment had been cooled down enough to allow the LNG that reached the pit to remain as a liquid, reducing its vaporization, and forming droplets on the concrete layer that continued to evaporate. The sudden increase in heat provided by the concrete surface is due to the formation of a permanent liquid layer, where the difference in temperatures was higher. At this point, the temperature of the concrete surface reached that of the liquid. The remaining of the filling and free evaporation operations showed a decrease in the heat transfer between the liquid and the concrete layers. This decrease was proportional to the difference in temperatures, which, as seen in Figure 21a (upper), was quite small due to the thermal equilibrium that has been achieved during the approximately 700 seconds of vaporization. As the pool was ignited at approximately 1700 seconds, no significant change in the slope of the heat transfer trend was observed, nor was there a change in the temperature of the concrete surface. Based on this observation, the lack of change in the trend is inferred to be due to the consumption of the radiative heat reaching the pool surface on the upper layers of the liquid pool, without affecting the heat transfer occurring at the bottom of the pool. This seems to indicate that the transmission of radiative heat from the lower layers of liquid to the concrete layer is not a possible mode for the utilization of the energy that reaches the pool. The previous statement is only a conjecture and until further testing no conclusions can be reached.

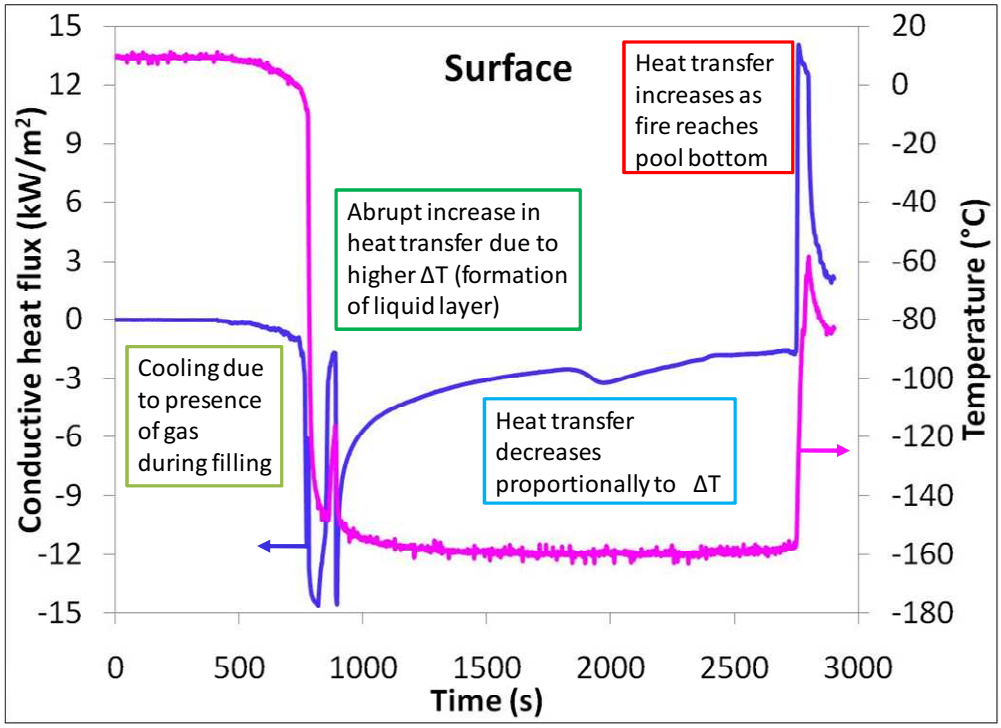

(a)

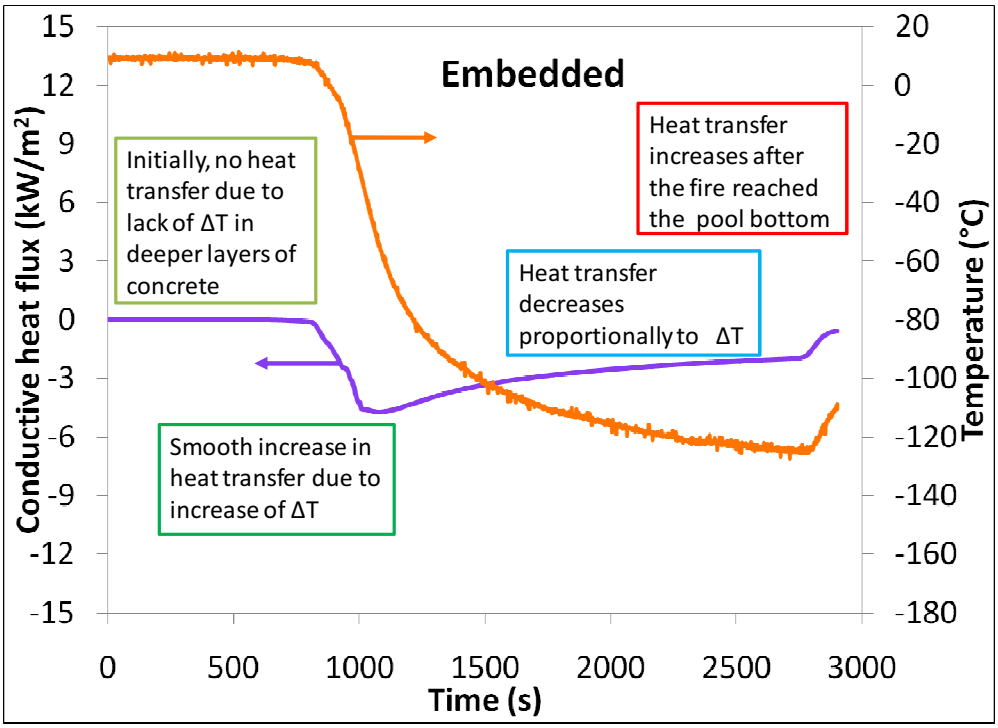

(b)

Figure 21. Conductive heat flux profile. (a) corresponds to the readings obtained from the heat flux sensor located on the concrete surface, and (b) corresponds to the readings obtained from the sensor located ½'' under the concrete surface

The final change in the heat transfer was due to the flame reaching the concrete surface because the liquid layer had disappeared and the temperature gradient between the concrete surface and the pool had achieved its larger point. This measured increment in temperature and heat flux was due to the radiative heat feedback from the flame. In Figure 21b, a similar trend can be observed in the heat transfer at the bottom of the pool during the filling, evaporation, and the burning periods. The main difference in this trend is the subtle changes seen in the heat transfer and temperature lines. This is due to the difference of temperature experienced at the measuring point, which was not exposed to extreme changes in temperature.

4.4.3 Radiometers

4.4.3.1 Radiometers outside the pit area

The data from the radiometers located downwind from the pit were used to obtain the average emissive power (SEP) of the flame. The radiometers were aimed at a fixed position in the lower section of the flames as seen in Figure 22. The solid flame model was used to calculate the SEP as mentioned in subsection 2.2.3, and the results (uncorrected for atmospheric absorption) are shown in Figure 23. The flame shape considered in the model corresponds to a vertical cylinder with a diameter equal to the equivalent diameter calculated as explained in subsection 2.2.1 and a height equal to that calculated by Thomas' correlation (see Table 4). The mass burning rate used in Thomas' correlation corresponds to the vaporization rate obtained with the differential pressure transducer as described in subsection 4.4.2 for method B (see Table 6).

Figure 22. Position of external radiometers

Figure 23 shows the radiation (purple and green lines) measured by the radiometer downwind from the pit area. These radiometers were located at 2 and 3 meters from the pit, respectively. As expected, the radiation received by the sensor closer to the pool fire was higher than that for the sensor located farther away. The SEP of the flame calculated based on the radiation data is also displayed in the plot (magenta and dark green lines). The darker green line was obtained with measurements from the radiometer located closer to the pit (~2m), and the magenta line was obtained with the measurements from the radiometer located approximately 3 m away from the pit (purple line). As mentioned above, these parameters are expected to have different magnitudes since they represent the heat emitted by the flame (SEP) and the radiant heat received by an object (q_r).

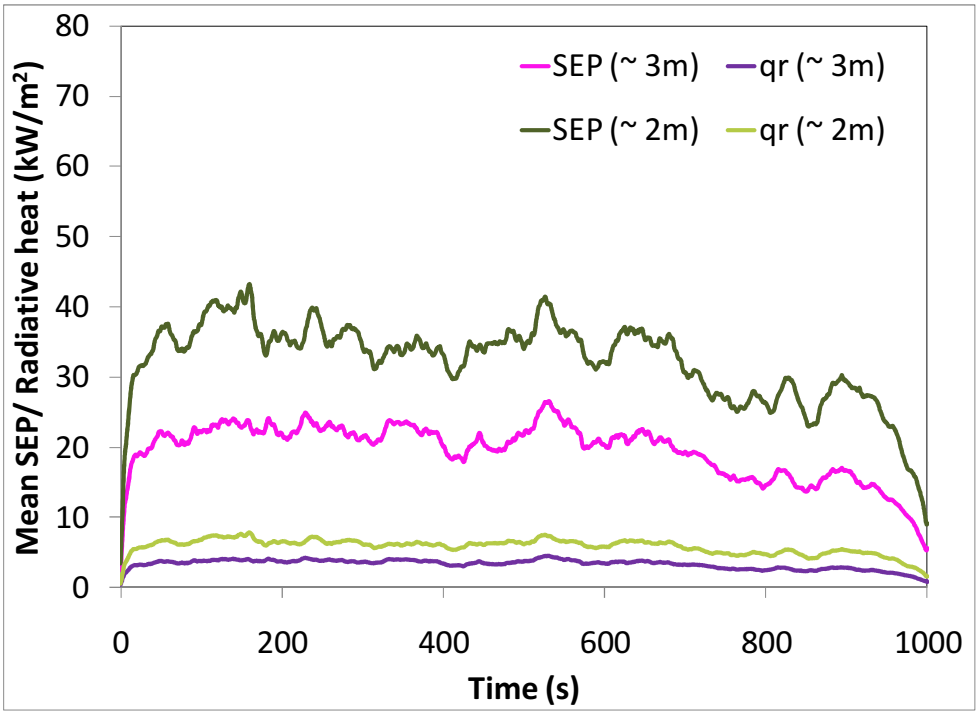

Figure 23. SEP values (dark green and magenta lines) and radiative heat fluxes (purple and green lines) reaching the surroundings

The average SEP of the flame calculated from the radiometer measurements was expected to give similar results since the radiation received by the sensor is related to the distance with respect to the source and the atmospheric absorption. However, as can be seen in the plot, the SEP obtained with the radiometer closer to the dike (dark green line) is higher than the SEP obtained from the radiometer located 1 meter behind it. The aim of the radiometer, the propagation of error inherent to the calculation of the SEP, and the assumptions of the model used are plausible explanations for the differences in the obtained values.

As can be seen in Figure 22, the radiometers were located at different positions, with different aims, and pointing towards different spots in the flame's base. Therefore, it is very likely that the view angles of the radiometers were not completely filled by the flame and a lower radiation value was potentially

measured. Furthermore, as stated by Moorhouse [38] the SEP calculated from radiation recordings depends on the surface area of the flame viewed by the recording sensor.

When the measured average SEP was compared to other SEP values with similar characteristics reported in the literature as seen in Figure 24, the SEP calculated in this work has a lower value than those typically found for LNG pool fires. The reason for this difference is likely due to the experimental conditions, with the other values shown from experiments of similar characteristics. Figure 24 includes a fitted curve for the data that attempts to represent the behavior of the mean SEPs of pool fires on land with increasing diameter. However, the main implications associated with the weakness of the trend line of the predicted behavior of the mean SEP values include the assumptions regarding the flame shape, the height of the flame, and the model used for its calculation. This is due to the uncertainty related to the details behind the calculations of SEPs values because of the limited information published.

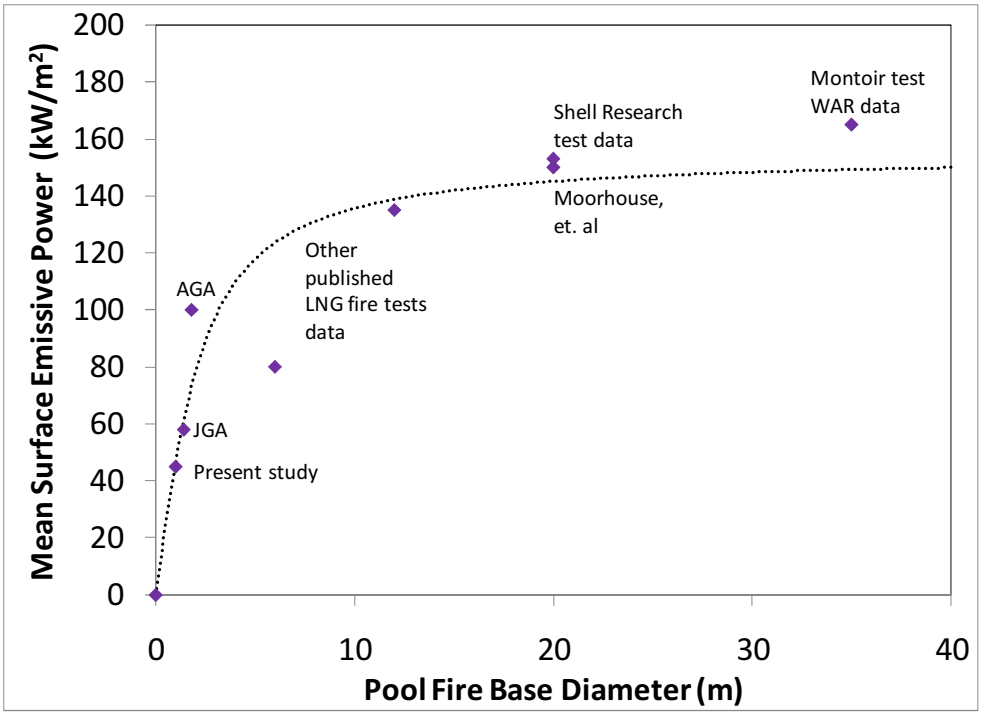

Figure 24. Variation of experimental SEP values of LNG pool fires on land with pool diameter (adapted and modified from [8])

4.4.3.2 Radiometers inside the pit area

The radiometers located inside the pit were initially intended to record the heat feedback to the liquid surface and to obtain an indirect calculation of the mass burning rate. However, as will be discussed later in this subsection, the recorded data could not be used for this and therefore supplementary analysis and conclusions were drawn.

The internal radiation obtained from the radiometers located inside the pit showed an initial peak in the heat feedback to the liquid pool as seen during the first seconds in Figure 25. As pointed out by Shinotake [39], the drop following the radical increase of radiation may be explained by a blockage occurring within the flame during the transient period. This blockage can be attributed to the accumulation of the combustion products in the lower sections of the flame or the unburned fuel vapors found above the liquid surface that obstructed the heat

feedback to the pool from the flame. This phenomenon did not influence the radiation captured by the radiometers outside the pit as seen in Figure 25.

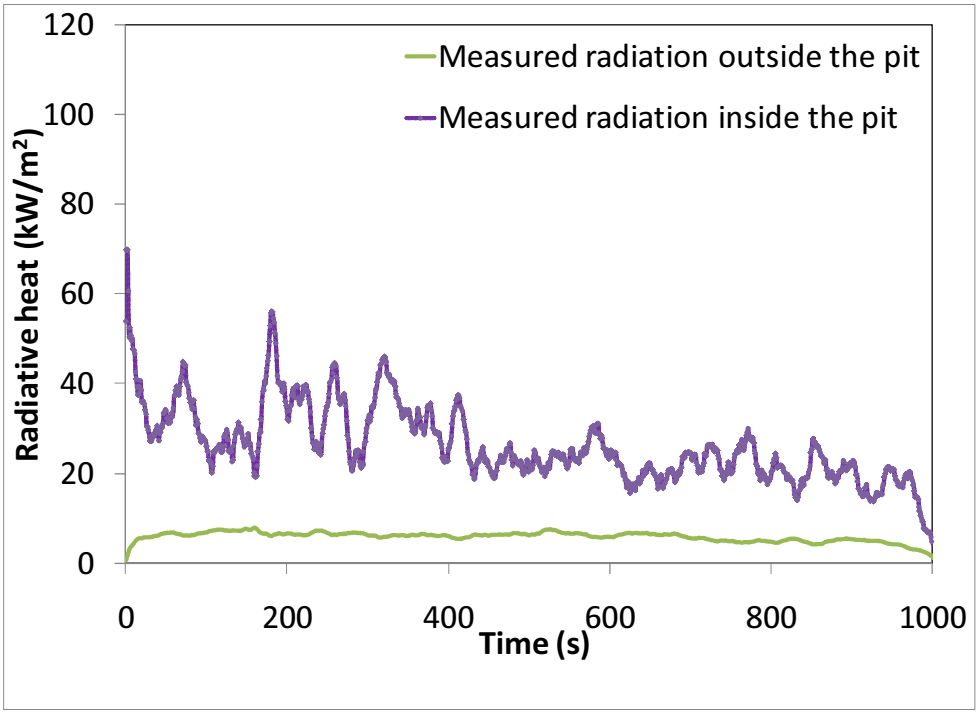

Figure 25. Comparison of the radiative heat fluxes measured inside and outside the pit

Even though initial observations seemed to point to the flame having low soot formation, Figure 26 shows differently. The soot accumulation on the window of the radiometers after the set of experiments was appreciable and seemed to indicate that this scale of experiments were optically thick fires instead of the expected optically thin fires. Nitrogen gas was used to avoid this phenomenon; however, nitrogen purge was stopped during the last test due to the long duration of the experiment.

Figure 26. Picture depicting the soot deposition on the radiometers used inside the pit area after the tests

Initially, the measurements of the radiative fluxes were intended to be used to calculate an average value for the mass burning rate. However, the heat flux feedback to the pool measured did not show a constant trend as expected and as exhibited by the mass burning rate. Therefore, when the energy balance was performed on the pool surface, the objective was to calculate the necessary radiative heat input to the pool for the given mass of LNG that was burned ($\dot{m}$). The goal of this calculation was to investigate the uncertainty in the behavior of the radiometer. For this calculation, the convective heat input to the pool was small enough to be neglected and the heat transfer to the bottom of the pool was not accounted for according to the results obtained from the heat flux sensors in subsection 4.4.2. Hence, the following expression was used:

$$q_r = \dot{m}\Delta H_v - q_{cond} \qquad 4\text{-}1$$

The heat of vaporization (ΔH_v) was taken as 510 kJ/kg, the heat conducted from the bottom of the pool (q_{cond}) was obtained from the heat flux

sensor on the concrete surface, and the LNG mass burning rate ($\dot{m}$) was taken from the results of method B (Table 6). The results are plotted in Figure 27.

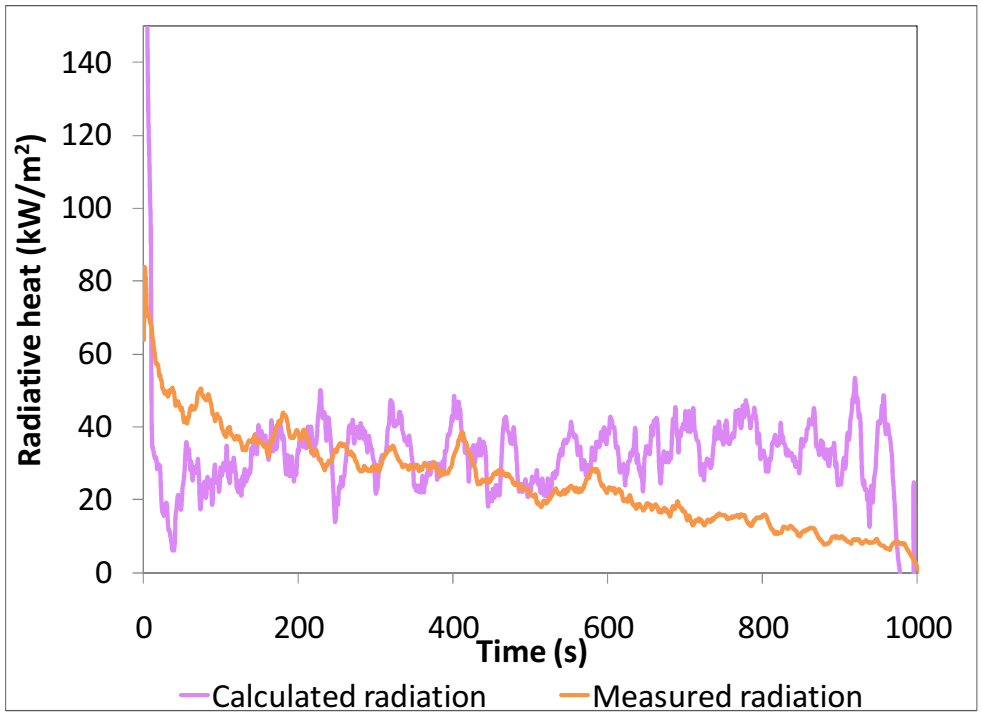

Figure 27. Comparison of the measured and calculated radiative heat flux received at the pool surface

The behavior of the measured radiation clearly exhibits a decreasing trend, which does not fit with the behavior seen in the mass burning rates, which, as mentioned above, was constant throughout the entire burning period. Possible explanations for this behavior are potential changes of the heat sink temperature in the sensor, possible accumulation of soot particles or water on the window, or possible alterations in the transmission of the signal. The first hypothesis seems plausible even though the sensor was cooled with water. If the heat sink temperature was to be variable and not constant, then the output of the sensor could give higher or lower radiative flux values according to the variation of the temperature. A decrease in the output signal requires an

increase in the heat sink temperature, which is credible due to the high temperatures of the flames that engulf the sensor during the burning period. The second possibility involves an unaccounted degree of interference with the readings by the thin layer of the particles deposited on the sensor. These particles were observed on the sensor's window after the experiments were performed. The latter premise may be due to the cryogenic temperatures that the signal cable was exposed to during the duration of the test. Even though, the former explanation is potentially the best reason for the variable behavior of the radiometer's output, qualitative tests were performed to obtain a better idea regarding the influence of any of these parameters.

The first qualitative test was performed in a lab setting to observe the influence of low temperatures on the output of the radiometer. To achieve this, the setup consisted of an infrared heat lamp posted at a vertical fixed height, a radiometer located in the center of a wood board, one thermocouple to record the temperature of the radiometer, and a bath of liquid nitrogen. We started by radiating the radiometer with the lamp for about 1000 seconds. Following this, the signal cable was submerged in the bath and we radiated the radiometer again for about 1500 seconds. This allowed us to determine if a change in the signal was significant enough to show the influence of the cryogenic temperatures in the radiometer signal. However, after analyzing the data recorded, we found that there was no significant change in the signal output to conclude that the immersion of the signal cable in a cryogenic bath affects the output of the sensor.

Following this, another qualitative test was performed to observe the effect of the temperature of the water cooling on the sensor's output by using the same setup as before. For this test, we used two different flow-in water temperatures, 21℃ and 40℃. The following three st eps (1000 sec each) describe the different stages of the experiment:

- First, the flow of ambient water was started. Following this, the lamp was lighted, the temperature of the water exiting was measured, and the radiometer's output was recorded. During the first stage, the temperature of the water exiting the radiometer was the same as the temperature entering it.
- After this, the flow of cooling water was stopped while recording of data continued. We observed that the output signal experienced an increase in noise.
- Finally, the flow of water at a higher temperature was initiated again. We observed that the flow of water stabilized the radiometer's signal at a lower value than the one recorded in the first stage.

From these observations, the most likely explanation is that the flow of cooling water was insufficient to maintain a constant sink temperature, resulting in the potential rise in the reference temperature of the sensor. Therefore, it is recommended that measurements of the cooling water temperature are made during the test.

Lastly, an attempt to estimate the radiative heat flux input to the pool was done by means of the thermocouple readings located at same height as each radiometer (described in subsection 3.3.1). The Stefan-Boltzmann equation was used to calculate the heat flux by assuming the flame as a black radiator, i.e., $\varepsilon = 1$ [40]:

$$q_r = \varepsilon\sigma(T_s^4 - T_{surf}^4) \qquad 4\text{-}2$$

The Stefan-Boltzmann constant σ was taken as $5.67*10^{-11}$ kW/m^{2}K^4, T_{surf} was assumed as the boiling temperature of the liquid pool receiving the radiation, and T_s the temperature of the flame, which is the body emitting the

energy. Figure 28 shows the results of the computed radiation along with the measured values.

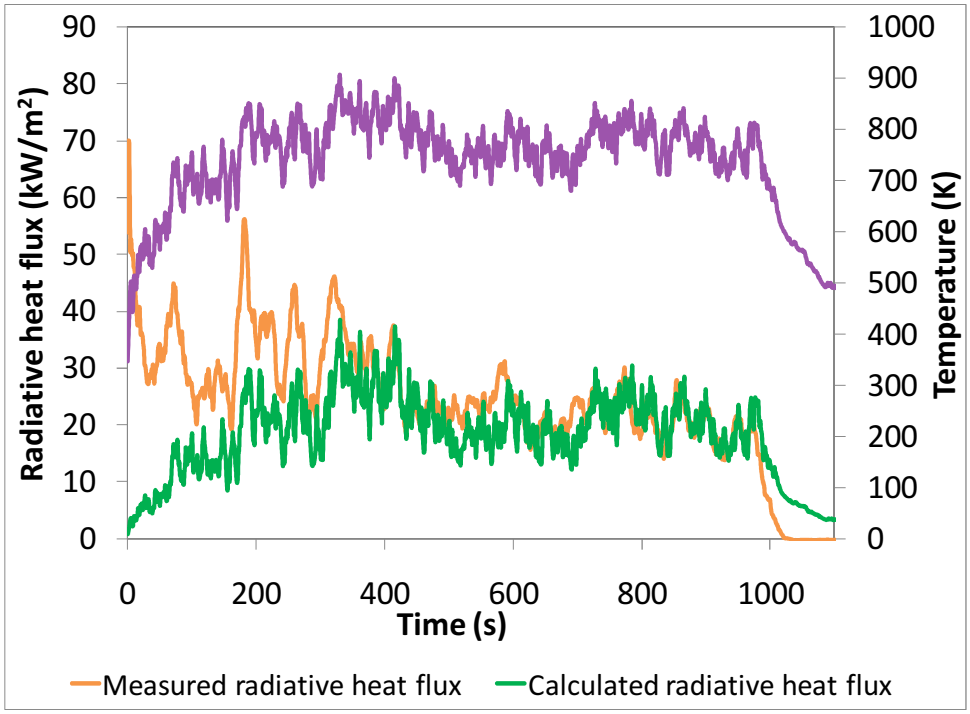

Figure 28. Calculated and measured radiative heat flux received at the center of the LNG pool surface. The purple line corresponds to the temperature measured at the same location of the radiometer

It is clear that the Stefan-Boltzmann law gave relatively good results after the initial 200 seconds. This law predicts the maximum radiation emitted by an ideal radiator. However, for our case, the T correspondes to the temperature measured by the thermocouple positioned at the radiometer site and not the equivalent average blackbody temperature, which is usually on the order of 1200K [41]. Consequently, the estimation of the radiative heat flux produced lower values that seemed to agree fairly well with the heat flux measured by the radiometer located in the center of the pool.

5. CONCLUSIONS AND RECOMMENDATIONS

5.1 Summary of conclusions

This subsection includes a summary of the findings that originated from the analysis of the set of experiments performed to study the measurement of mass burning rates of LNG pool fires. The analysis of the gathered data was also used to identify characteristic parameters of a fire, such as flame height, tilt angle, emissive power, and radiative heat flux. The following summarizes the key findings:

- Wind speeds influence the shape of the flame. However, the speeds experienced during the tests were quite low and did not significantly affect the shape of the flame. This was further proven by the similarities in the flame height and flame length.
- The semi-empirical correlations commonly found in the literature to predict flame geometry characteristics such as flame height and tilt seemed to work well as rough estimates for tests on a small scale.
- The semi-empirical correlations used for the prediction of mass burning rates produced estimates that were on the same order of magnitude with the measured rates and those from previous experiments. It was noticed that caution needs to be exerted for the prediction of burning rates of small scale LNG pool fires.
- The validity of the commonly used methods to measure LNG mass burning rates was confirmed by comparison of the results from three different techniques.
- The measurements of the heat transfer at the bottom of the pool, between the concrete layer and the liquid pool, showed that radiative heat reaching the pool surface was not lost due to transmission to the concrete surface.

- The emissive power of the flame calculated from the radiative heat flux measured outside the pit provided low values compared with the values found in the literature. This was attributed to the direction of the radiometer and the variance of the emissive power over the surface area of the flame, which is assumed as a constant value during the calculation.

During the analysis of the evaporation of LNG due to the heat feedback from the flame, a number of problems were encountered with the radiometer data. This included an instrumentation problem during the first experiment, off-scale measurements during the decay of the flame, incomplete coverage of the flame by the view (aim) of the radiometer, and possible condensation of water or alteration of the reference temperature of the radiometer due to exposure to cryogenic temperatures for extended periods of time.

5.2 Recommendations for future research

It was observed that reliable measurements in turbulent flames are quite challenging and difficult to make. This is mainly due to the limitations encountered in reproducing experimental conditions and in isolating variables without affecting the realism of the experiment. The performance of this set of experiments revealed a number of aspects that we recommend to be further studied to move forward in this research area and to reduce the problems encountered with the acquired data. This includes:

- Study the heat transfer at the bottom of the pool as well as at the container's walls in order to obtain more data that will aid in the characterization of the vaporization of the LNG mass.
- Track the temperature of the water cooling used in the radiometers inside the flame to obtain an indirect measurement of the sensor's reference temperature and its influence on its output.

- Increase the flow of the nitrogen purge to decrease the soot deposition on the sensor's window.

The series of tests presented in this work were performed in a small scale scenario. Future efforts to study the relation of the radiative heat feedback and the mass burning rates should include a series of tests in larger scales with variable pool depths. This would provide more information regarding the dependence of the transmission of energy on the depth of the liquid layer and would avoid the need for extrapolation of the results.

Finally, a series of experiments in a laboratory setting where conditions such as convective heat and radiative heat feedback can be controlled is recommended to be carried out to expand the information collected to study the burning rates of LNG. The objective of this type of work is the fundamental study of the absorption characteristics of LNG due to thermal radiation. The information obtained can be used to validate the results obtained during the small scale experiments where thermal radiation was not observed reaching the bottom of the pool.

REFERENCES

[1] Center for Liquefied Natural Gas (CLNG), http://www.lngfacts.org, accessed in December 2010.

[2] U.S. Energy Information Administration (EIA), http://www.eia.doe.gov, accessed in January 2011.

[3] C.D. Zinn, LNG codes and process safety, Process Safety Progress 24 (2005) 158-167.

[4] Committee for the Prevention of Disasters (CPD), Methods for the Calculation of Physical Effects Due to Releases of Hazardous Materials (liquids and gases): Yellow Book, Third edition, CPD, The Hague, (2005).

[5] National Fire Protection Association (NFPA), Standard for the Production, Storage, and Handling of Liquefied Natural Gas (LNG), Quincy, MA, NFPA, (2001).

[6] Code of Federal Regulations, 49-Transportation, Subchapter D: Pipeline Safety, Part193, Liquefied Natural Gas Facilities, Federal Safety Standards, (1986).

[7] H. Malvos, P. Raj, Thermal emission and other characteristics of large liquefied natural gas fires, Process Safety Progress 26 (2007) 237-247.

[8] P.K. Raj, LNG fires: A review of experimental results, models and hazard prediction challenges, Journal of Hazardous Materials 3 (2007) 444-464.

[9] H. Malvos, Details of 35 m diameter LNG fire tests conducted in Montoir, France in 1987, and analysis of fire spectral and other data, AIChE Spring National Meeting, April 23-27, Orlando, FL, (2006), 1-20.

[10] D. Nedelka, J. Moorehouse, R.F. Tucker, The Montoir 35m diameter LNG pool fire experiments, Ninth International Conference & Expo on LNG, 17-20 October, Nice, France, (1989).

[11] P.K. Raj, LNG pool fire spectral data and calculation of emissive power, Journal of Hazardous Materials, 142 (2007) 720-729.

[12] A. Luketa-Hanlin, A review of large-scale LNG spills: Experiments and modeling, Journal of Hazardous Materials 132 (2006) 119-140.

[13] P. Raj, Large hydrocarbon fuel pool fires: Physical characteristics and thermal emission variations with height, Journal of Hazardous Materials, 140 (2007) 280-292.

[14] Fire Dynamics Tools (FDTs) Quantitative Fire Hazard Analysis. Methods for the U.S. Nuclear Regulatory Commission Fire Protection Inspection Program, NUREG-1805, United States Nuclear Regulatory Commission, (2004).

[15] K.B. McGrattan, H.R. Baum, A. Hamins, Thermal radiation from large pool fires, NISTIR 6546, National Institute of Standards & Technology, US Department of Commerce, Washington, DC, (2000).

[16] P. Joulain, The behavior of pool fires: State of the art and new insights, Symposium (International) on Combustion 27 (1998) 2691-2706.

[17] B.J. McCaffrey, Purely Buoyant Diffusion Flames. Some Experimental Results, NBSIR-79-1910 Center for Fire Research, National Bureau of Standards, (1979).

[18] P. Raj, Large LNG fire thermal radiation-modeling issues and hazard criteria revisited, Process Safety Progress 24 (2005) 192-202.

[19] P.H. Thomas, The size of flames from natural fires, Symposium (International) on Combustion 9 (1963) 844-859.

[20] American Gas Association (AGA), LNG safety research program interim report on phase II work, Report IS-3-1, Battelle Columbus Laboratories, Arlington, VA, (1974).

[21] J. Welker, C. Sliepcevich, Bending of wind-blown flames from liquid pools, Fire Technology 2 (1966) 127-135.

[22] V. Babrauskas, Estimating large pool fire burning rates, Fire Technology 19 (1983) 251-261.

[23] K.S. Mudan, Thermal radiation hazards from hydrocarbon pool fires, Prog. Energy Combust. Sci. 10 (1984) 59-80.

[24] M. S. Mannan, Lees' Loss Prevention in the Process Industries, Volumes 1-3, 3rd Edition, Elsevier,U.S., (2005).

[25] H. Hottel, A. Sarofim, Radiative Transfer, McGraw-Hill, New York, (1967).

[26] The SFPE Handbook of Fire Protection Engineering, Society of Fire Protection Engineers, NFPA, Quincy, MA, (1988).

[27] V.I. Blinov, G.N. Khudiakov, Diffusion burning of liquids, English translation: U.S. Army Engineering Research and Development Laboratories, Information Resources Branch, Translattion analysis Section, NTIS No. AD296762, Fort Belvoir, VI, (1961).

[28] H.C. Hottel, Certain laws governing diffusive burning of liquids, Fire Research Abstracts and Reviews 1 (1959) 41-44.

[29] M.G. Zabetakis, D. S., Burgess, Research on the hazards associated with the production and handling of liquid hydrogen, Bureau of Mines Report of Investigations 5707, Washington, DC, (1961).

[30] J.M. Chatris, J. Quintela, J. Folch, E. Planas, J. Arnaldos, J. Casal, Experimental study of burning rate in hydrocarbon pool fires, Combustion and Flame 126 (2001) 1373-1383.

[31] D. Burgess, A. Strasser, J. Grumer, Diffusive burning of liquid fuels in open trays, Fire Research Abstracts and Reviews, Pittsburg, PA, 3 (1961) 91-106.

[32] H. Koseki, Combustion properties of large liquid pool fires, Fire Technology 25 (1989) 241-255.

[33] W.G. May, W. McQueen, Radiation from large liquefied natural-gas fires, Combustion Science and Technology 7 (1973) 51-56.

[34] G.A. Mizner, J.A. Eyre, Large scale LNG and LPG pool fires, Inst. Chem. Eng. Symp., April, Manchester, 71 (1982) 147-163.

[35] A. Hamins, S.J. Fischer, T. Kashiwagi, M.E. Klassen, J.P. Gore, Heat feedback to the fuel surface in pool fires, Combustion Science and Technology 97 (1994) 37 - 62.

[36] D. Rall, Heat Flux, (1972).

[37] B.N. Taylor, C.E. Kuyatt, Guidelines for evaluating and expressing the uncertainty of NIST measurement results, NIST Tech. Note 1297, U.S. Goverment Printing Office, Washington, DC, (1993).

[38] J. Moorhouse, Scaling criteria for pool fires derived from large-scale experiments, Institution of Chemical Engineers, Symposium Series 71, Manchester (1982), 165-179.

[39] A. Shinotake, S. Koda, K. Akita, An experimental study of radiative properties of pool fires of an intermediate scale, Combustion Science and Technology 43 (1984) 85-97.

[40] F.P. Incropera, D.P. Dewitt, T.L. Bergman, A.S. Lavine, Fundamentals of heat and mass transfer 6th ed., John Wiley, Hoboken, NJ, (2006).

[41] S. Atallah, D. Allan, Safe separation distances from liquid fuel fires, Fire Technology 7 (1971) 47-56.

APPENDIX A

Temperature profile for test 1

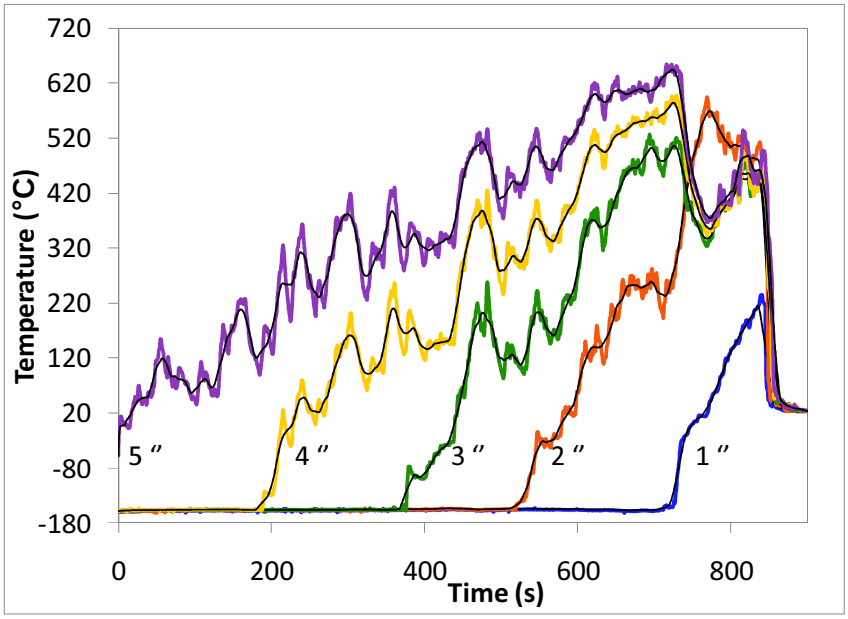

(a)

LNG level profile and mass burning rates behavior for test 1

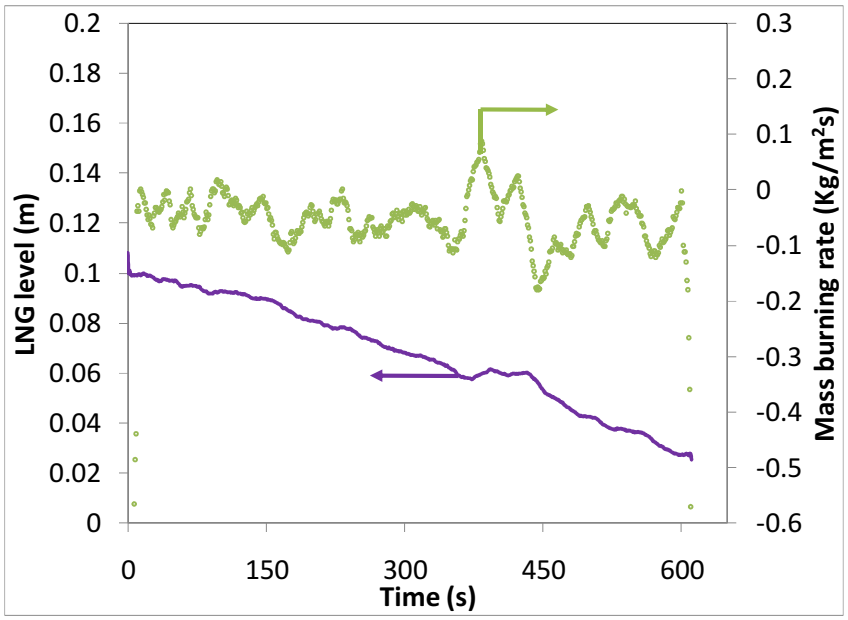

(b)

Level profile for test 1

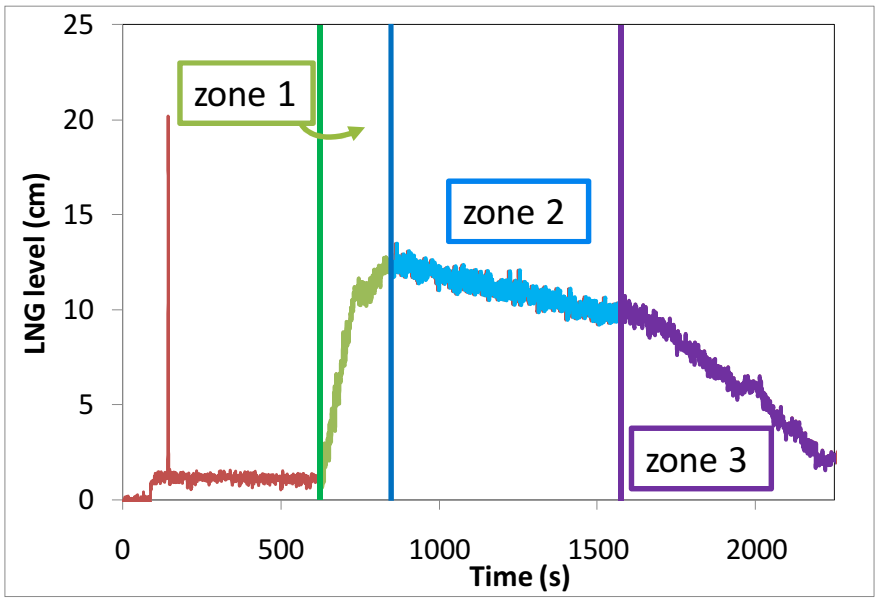

(c)

Radiative heat flux profile measured at the pool surface for test 1

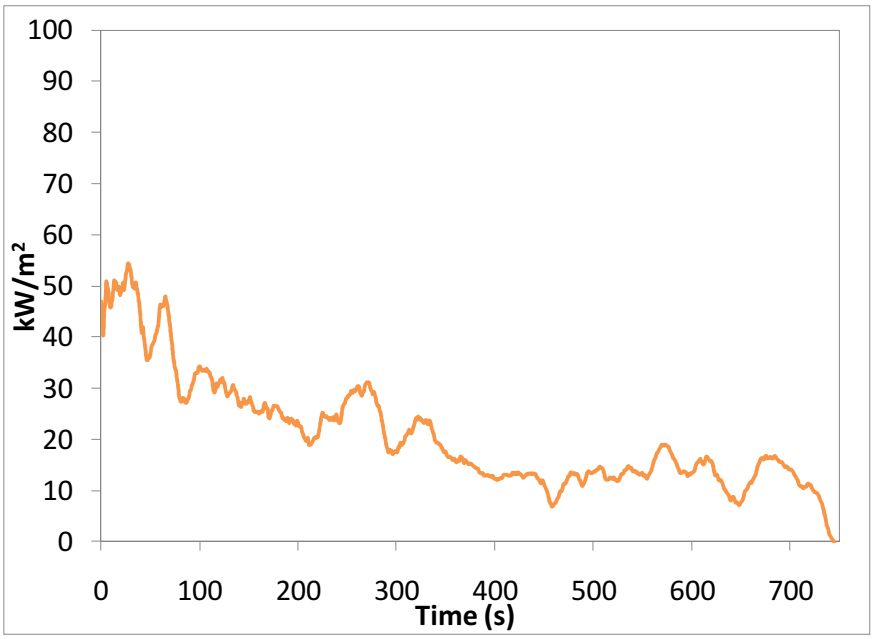

(d)

Heat flux profile for test 1

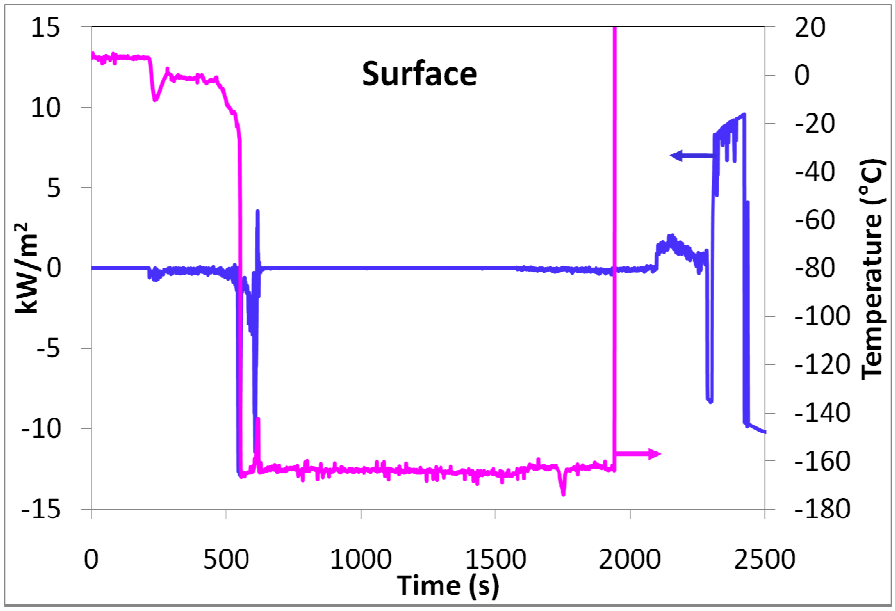

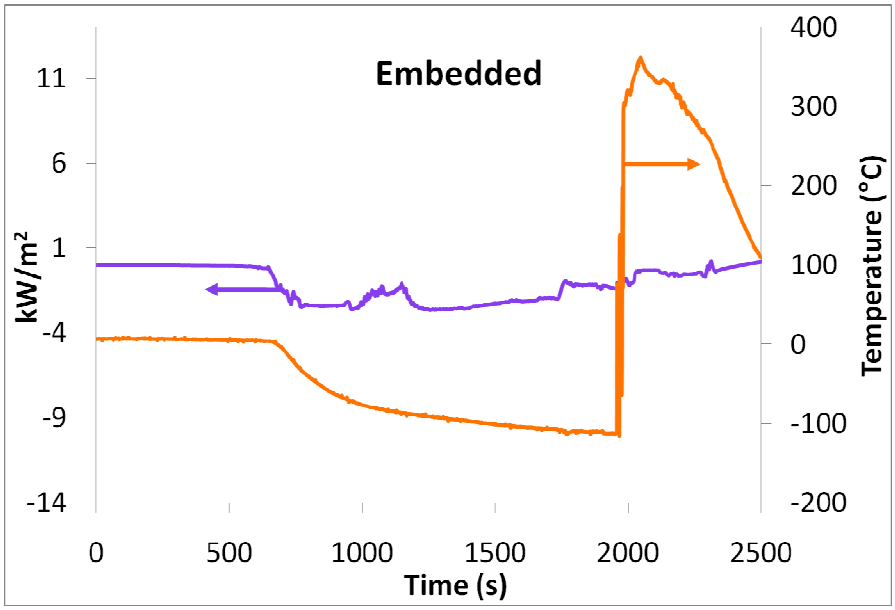

(e)

Temperature profile for test 3

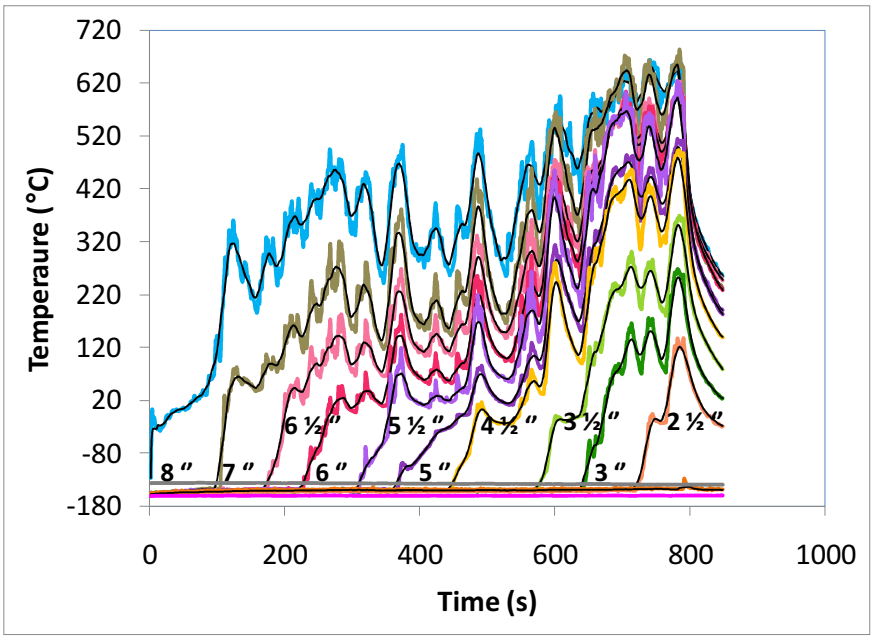

(f)

LNG level profile and mass burning rates behavior for test 3

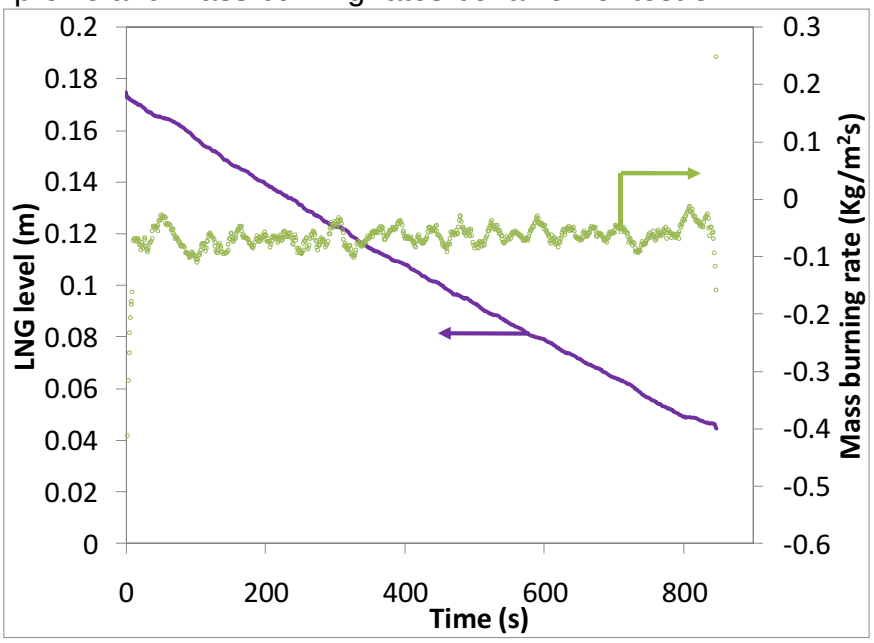

(g)

Level profile for test 3

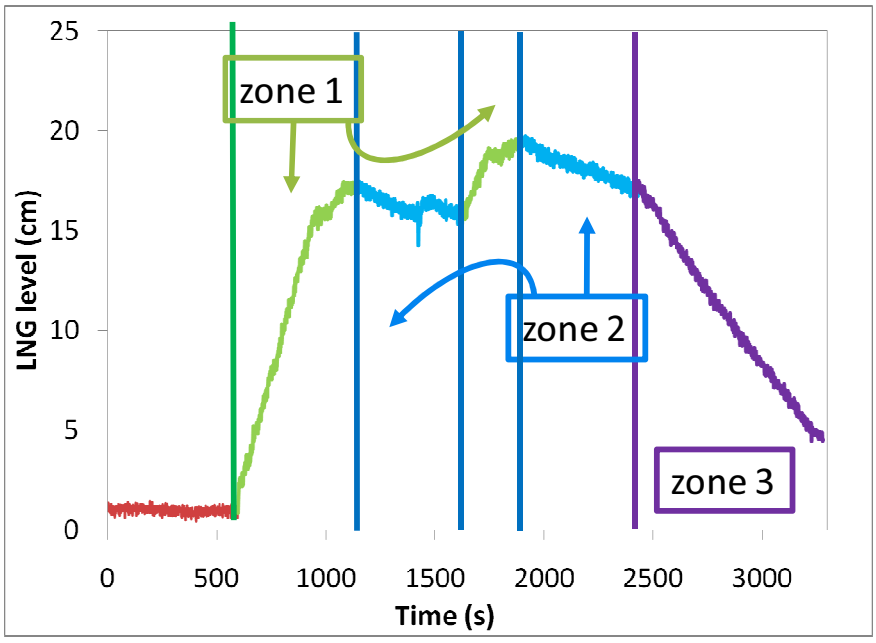

(h)

Radiative heat flux for test 3

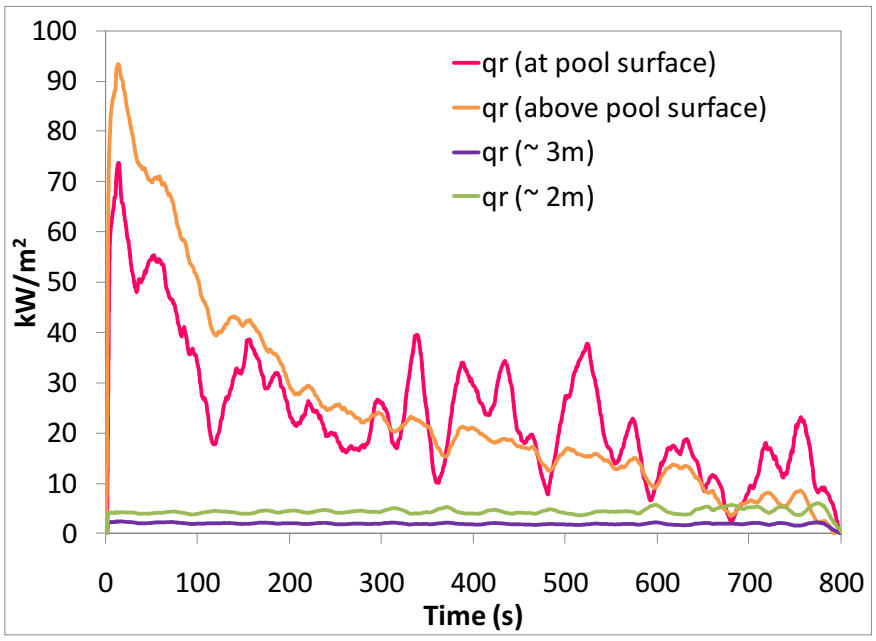

(i)

Visible flame height & length for test 3

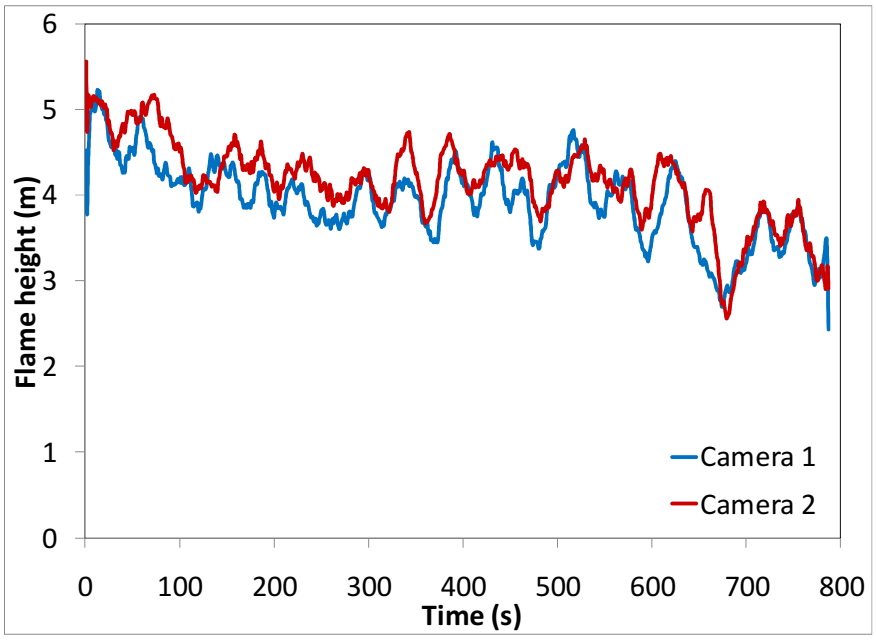

(j)

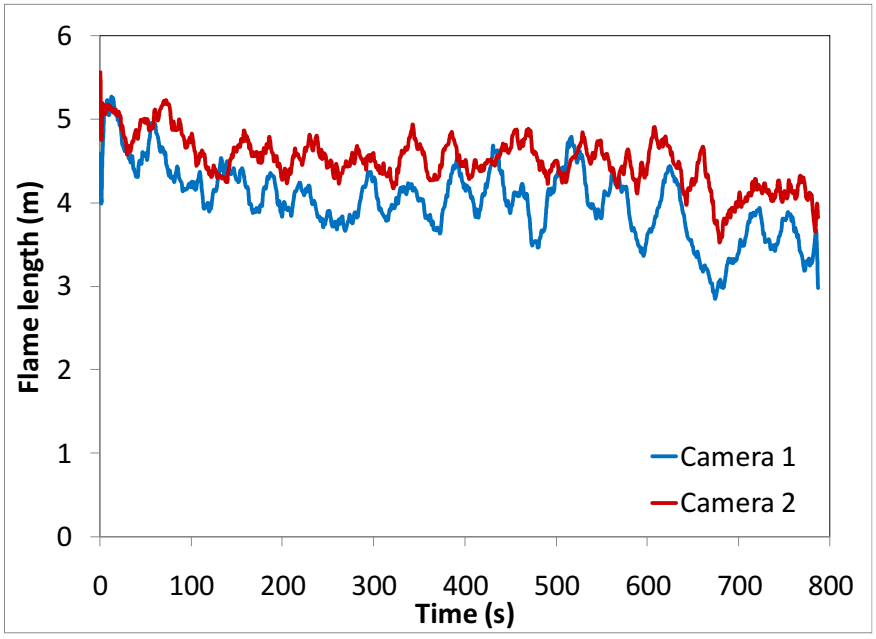

(k)

Heat flux profile for test 3

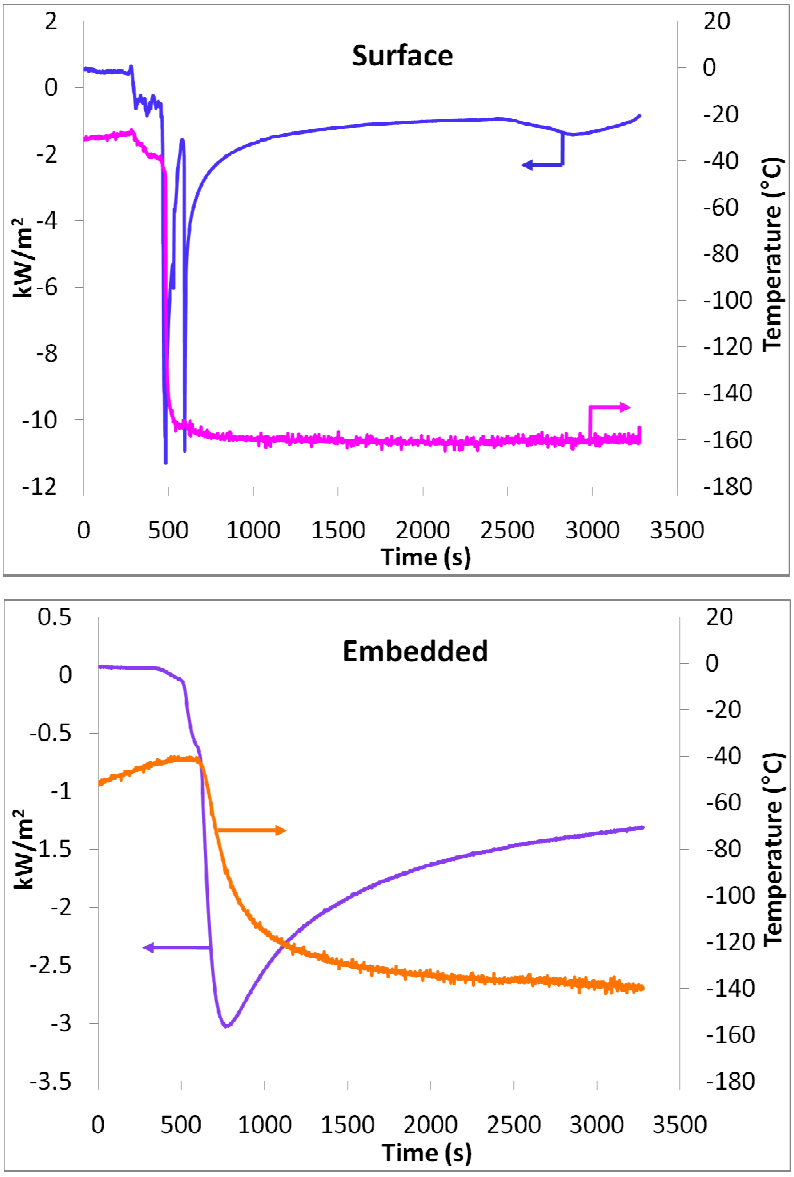

(l)

Table A. Display the R square values for the line fitting

Test	R square
1	0.969
2	0.997
3	0.996

VITA

Name: Lady Carolina Herrera Gómez

Address: Mary Kay O'Connor Process Safety Center
3122 TAMU
College Station, TX 77843-3122

Education: B.S., Chemical Engineering, Universidad Industrial de Santander, 2006
M.S., Safety Engineering, Texas A&M University, 2011